Changes in Tissue Protein *N*-Glycosylation and Associated Molecular Signature Occur in the Human Parkinsonian Brain in a Region-Specific Manner

Ana Lúcia Rebelo[1], Richard R. Drake[2], Martina Marchetti-Deschmann[3], Radka Saldova[1,4,5], Abhay Pandit[1]*

[1]SFI CÚRAM Research Centre for Medical Devices, National University of Ireland Galway, Ireland

[2]Department of Cell and Molecular Pharmacology and Experimental Therapeutics, Medical University of South Carolina, Charleston, USA.

[3]Institute of Chemical Technologies and Analytics, Vienna University of Technology, Vienna, Austria.

[4]National Institute for Bioprocessing Research and Training (NIBRT), University College Dublin, Ireland

[5]School of Medicine, College of Health and Agricultural Science, University College Dublin, Ireland

*Abhay Pandit, abhay.pandit@nuigalway.ie

KEYWORDS: Parkinson's disease, *N*-glycosylation, protein glycosylation, glycomics, human brain, striatum, substantia nigra, ER stress

ABSTRACT (150 words)

Parkinson's Disease (PD) associated state of neuroinflammation due to the aggregation of aberrant proteins is widely reported. One type of post-translational modification involved in protein stability is glycosylation. Here, we aimed to spatially characterise the human Parkinsonian nigro-striatal *N*-glycome, and related transcriptome/proteome, and its correlation with endoplasmic reticulum stress and unfolded protein response (UPR), providing a comprehensive characterisation of the PD molecular signature.

Significant changes were seen upon PD: 3% increase in sialylation and 5% increase in fucosylation in both regions, and 2% increase in oligomannosylated *N*-glycans in the substantia nigra. In the latter, a decrease in the mRNA expression of sialidases and an upregulation in the UPR pathway were also seen.

This complete characterisation of the human nigro-striatal *N*-glycome provides an insight into the glycomic profile of PD through a transversal approach while combining the other PD "omics" pieces, which can potentially assist in the development of glyco-focused therapeutics.

INTRODUCTION

Parkinson's Disease (PD) is characterised by the death of dopaminergic neurons in the substantia nigra pars compacta due to the presence of Lewy Bodies composed of protein aggregates, leading to neurodegeneration[1]. Despite the increased knowledge and pathway-oriented research regarding PD pathophysiology, the study of how glycosylation in the brain correlates with the progression of the disease remains overlooked. Glycosylation is the major highly-regulated post-translation modification of proteins, modulating the protein's function, structure and conformational stability[2]. Since PD is associated with aberrant aggregation of α-synuclein, and as glycosylation affects proteins' structure and function, studying this feature is highly attractive.

N-linked glycans are the most common type of glycans in eukaryotic glycoproteins, since around 90% of these glycoproteins carry them[3]. *N*-glycans can be categorized into three groups: oligomannose (only mannose residues are linked to the core structure); complex (branched structures are attached to the core); and hybrid (only mannose residues are linked to the Man-α-(1,6) arm of the core and one/two branches starting with a GlcNAc residue are on the Man-α-(1,3) arm)[4]. Their ubiquity and implication in every biological process highlights their importance. In the central nervous system (CNS) they play essential roles in differentiation, synaptogenesis, neurite outgrowth and myelinogenesis during development[5]. Congenital disorders of glycosylation (CDGs) are associated with different neuropathological symptoms such as seizures and stroke-like episodes[6], highlighting how glycan dysregulations can affect the CNS.

N-glycosylation takes place within the Endoplasmic Reticulum (ER) and the Golgi apparatus, involving various glycosidases and glycosyltransferases that participate in the formation and trimming of the different glycosidic chains[7,8] and chaperones to promote proper folding of the proteins. At the same time, a strict quality control system occurs by the glucosyltransferase uridine diphosphate glucose (UGGT) in the ER. This recognises any misfolded glycoproteins (which could be due to aberrant *N*-glycosylation) and either promotes their re-glycosylation until proper folding or targets them for degradation[9–11]. It is also in the ER that the first step in the assembly of *N*-glycans takes place,

where the newly-formed glycan chain is transferred from a lipid-linked oligosaccharide to the asparaginyl residues of the new glycoprotein's precursors, which is catalysed by an oligosaccharyltransferase[2]. The presence of metabolic deficiencies affecting this process, such as tunicamycin administration, has been described to be compensated by ER stress responses[12][13]. To decrease ER stress and inhibit the accumulation of misfolded proteins, the unfolded protein response (UPR) takes place, being activated through three different signal transducers: protein kinase-like ER kinase (PERK), protein kinase inositol requiring kinase 1 (IRE1) and activation transcription factor 6 (ATF6)[14]. On the other hand, (an) insufficient ER stress response has been correlated with (an) increased susceptibility of mouse cerebellar neurons to *N*-glycosylation defects[15], emphasizing the bidirectional relationship between *N*-glycosylation and ER homeostasis[16]. Thus, there are multiple players whose actions must be taken into account when characterising the healthy vs diseased environment.

This study represents a comprehensive spatio-temporal analysis of the human nigro-striatal protein *N*-"glyco" profile to understand how it is modulated along with other molecular players in PD (**Figure 1**). Since glycosaminoglycans (GAGs) and *O*-glycome have recently been characterised in PD[17,18], we explore the missing puzzle pieces to complete the characterisation of protein glycosylation upon the onset of PD. This overview of the PD "-omics" is relevant since it allows for a more encompassing investigation of the modulation of *N*-glycosylation upon disease and how it interacts transversely with the overall molecular signature in the brain.

RESULTS

Specific glycosylation traits changes are seen in the overall glycome upon PD progression

To assess the alterations happening in the overall glycome, a high throughput screen was performed using a lectin microarray (**Figure 2**). A high presence of mannose residues, multi antennary *N*-glycans, GlcNAc oligomers, terminal galactose, alpha(2,6)-linked sialic acids and fucosylated glycans was detected across the groups and in both regions. Surprisingly, a low amount of Tn antigen (GalNAc-α-O-Ser/Thr) was also present, which is usually lacking in healthy cells but has been reported in the serum of Alzheimer's disease (AD) patients and their age-matched controls[19]. Significant differences were detected in the binding intensity of some of these lectins, which translates into a different expression of some glycans. In the striatum, a significant decrease was seen in the binding of AAA (outer arm fucose) and PWA (branching). On the other hand, in the substantia nigra there is a significant decrease in mannosylation (ASA, GNA), GlcNAc groups (DSL, LEL, PA-I), galactosylation/poly-LacNAc groups (RCA, CAL) as well as core fucosylation, which suggests that a decrease in complexity occurs. The binding of SNA and MAA did not express significant differences in disease in either of the regions.

Lectin histochemistry for ricinum communis agglutinin (RCA), galanthus nivalin agglutinin (GNA), datura stramonium (DSL), sambucus nigra agglutinin isolectin-I (SNA), anguilla anguilla agglutinin (AAA) combined with immunohistochemistry for the main inflammatory-related cells (astrocytes and microglia) was performed to assess the spatial distribution of the different glycans (**Figure 2**). Some of these correlated with astrocytes, but they were mainly binding to either extracellular matrix, or other cell types (potentially neurons).

N-Glycome profile of the healthy human nigro-striatal regions is mainly composed of galactosylated, highly fucosylated and oligomannosylated structures

After looking at the overall glycosylation traits, a more in-depth study of the *N*-glycosylation patterns was performed. For this, a combination of hydrophilic interaction liquid chromatography – ultra performance liquid chromatography (HILIC-UPLC) and liquid chromatography-mass spectrometry (LC-MS) was used after assessing the reproducibility of the results with control samples (**Figure S1).** The combination of both approaches enabled the) identification and quantification of both low- and high-abundance of over 120 *N*-glycan isomers for both striatum and substantia nigra spread over 59 glycan peaks (GP) **(Table S6, Table S7)** (main glycan structures seen in each GP are described in **Figure 3**).

To analyse the distinct traits, the major glycan constituent of each peak was considered the representative feature of that peak and the main traits were calculated by adding the abundance of the peaks where the main glycan expressed shared the same structural feature (**Table S1)**. The glycoproteins in the healthy striatum and substantia nigra were seen to carry a high percentage of galactosylated and core fucosylated structures (around 47% each). Additionally, approximately 81% of the total *N*-glycans are neutral in the striatum, whereas in the substantia nigra this value drops to around 73%. From the sialylated glycans, only about 2% and 5% contain polysialic acid in the striatum and substantia nigra, respectively (**Figure 4**). The abundance of bisected glycans is lower (around 14% in the striatum and 11% in the substantia nigra). Most of the glycans are also branched (approximately 68% in both regions) indicating a high complexity in the structures present in the nigrostriatal pathway (**Figure 4**).

Interestingly, alpha-galactose epitopes (Gal-α1-3-Gal) were detected (both by HILIC-UPLC and lectin array). However, since humans cannot synthesise this residue as they lack the enzyme α1,3galactosyltransferase, this is most probably of non-human origin, being possibly contamination or due to dietary residues.

Parkinsonian brains display region-specific alterations in *N*-Glycosylation traits compared to the healthy ones

The main glycosylation traits were analysed individually to compare the *N*-glycome between healthy, ILBD and PD in both regions (according to **Table S1**). The analysis by traits rather than by individual structures is crucial since the different glyco-moieties of glycoproteins play distinct roles in facilitating the recognition, binding and processing through the different receptors on cell membranes.

In both regions the abundance of neutral glycans remained similar in healthy and incidental Lewy bodies disease (ILBD), decreasing significantly in the later stages of the disease (**Figure 4**). Polysialic acids were significantly increased by 1.6-fold in the striatum upon disease; however, the opposite trend was seen in the substantia nigra (11% reduction).

Concerning oligomannosylation, in the two regions analysed the trends seen were contrasting: in the striatum the abundance of oligomannose structures seems constant between healthy and the ILBD group, decreasing significantly at the later stages of the disease. However, in the substantia nigra there is a decrease in the presence of these glycans upon ILBD, and an increase at the later stages of the disease (**Figure 4**).

As for fucosylation, in both regions a significant increase in both core and outer arm fucosylation between healthy controls and later stages of PD was seen (in the striatum, 1.09-fold increase in core fucose and 1.28-fold increase in outer arm fucose, whereas in the substantia nigra 1.12-fold increase in core fucose and 1.19-fold increase in outer arm fucose were seen). In the substantia nigra there is a significant increase in both types of fucosylation in the ILBD group, which suggests that fucose expression occurs in parallel with the progression of the disease. On the other hand, the expression of galactose residues in the *N*-glycan structures present both in the striatum and substantia nigra increases significantly upon PD (1.01-fold and 1.11-fold, respectively). Interestingly, there is a significant increase in mono-galactosylated structures in both regions (1.30-fold and 1.38-fold respectively), while the tri- and tetra- galactosylated ones decrease in the striatum (21% and 32% reduction, respectively) and increase in the substantia nigra (1.28-fold and 1.20-fold respectively).

As with the tendencies seen in the other glycosylation traits, the trends in the abundance of bisected *N*-glycans change between the two regions studied: in the striatum, there is a significant increase in the percentage of total bisects upon PD, whereas in the substantia nigra, these are significantly downregulated (**Figure 4**).

Regarding the branched structures, *N*-glycans with two branches are significantly increased in the striatum (1.31-fold increase), whereas they decrease in the substantia nigra (22% reduction). However, glycans with three branches are upregulated in both regions. Structures with four antennae are sharply decreased in the striatum and increased in the substantia nigra. Also, there are no significant changes between the healthy and ILBD groups in either the bisected or the branched glycans.

Individual N-glycans' identification, validation, and spatial distribution were assessed through MALDI mass spectrometry imaging (MALDI-MSI). This revealed a decreased expression of specific structures in PD brains compared to healthy ones, corroborating the significant differences already determined by HILIC-UPLC. This was the case of M3, M4, M5 and FA2F1G1 (which correspond to GP1, GP3, GP17 and GP13, respectively, on the HILIC-UPLC data) in the striatum (**Figure 5).** Another structure (FM5A1) was shown to be downregulated in PD brains through MALDI-MSI; however, this was not detected through HILIC-UPLC. This contributes to the decrease in oligomannosylation seen upon disease in the striatum. Similarly, in the case of the substantia nigra, downregulation in the expression of some oligomannose structures was also seen, mainly of M3, M4 and M7, corresponding to GP1, GP3 and GP17, respectively (**Figure 5).** A decrease in FA3F1G1 (GP15) is also seen through MALDI-MSI, and the presence of another structure (M9Glc1 – increased upon PD), which was not previously detected through HILIC-UPLC. This indicates that even though there is an overall increase in oligomannosylation in the substantia nigra upon disease, the abundance of some specific structures from this glycosylation trait is decreased. Other structures were detected; however, significant changes were not seen using this technique.

The results seen highlight the possibility of using this technique not only to validate the previous data, but also to assess its spatial distribution within the different regions in the striatum and substantia nigra. Furthermore, this also allows the previous data to be complemented through the detection of structures that were not deciphered previously by HILIC-UPLC and LC-MS.

Regulation of glyco-enzymes transcripts and expression is region- and disease-dependent

As previously mentioned, glycosylation of proteins is a non-template-driven mechanism that depends upon the action of multiple *glyco*-enzymes[2]. Therefore, an assessment of the changes in their transcription and expression is of significance.

In the substantia nigra of PD patients, significant downregulation was mainly seen in *N*-acetylgalactosaminyltransferases (GANTL-5, -9, -11, -14, which are predominantly involved in *O*-glycosylation, were decreased by -14.65-fold, -3.64-fold, -3.91-fold and -8.59-fold, respectively), in *N*-acetylglucosaminyltransferases (MGAT-4B, -4C, -5B, which play a role in the branching of *N*-glycans), in sialidases (NEU-1, -2) and sialyltransferases (ST8SIA-3, -4, -6, which are mainly regulating the formation of poly-sialic acids). There was also a -3.75-fold significant decrease in GLB1, a galactosidase involved in the different types of protein glycosylation and in the processing of gangliosides, more specifically GM1, which has been reported to be reduced in PD brains[20](**Figure 6**).

In the striatum, only one gene in PD was significantly downregulated - B3GNT4 (-8.69-fold reduction), an *N*-acetylglucosaminyltransferase responsible for the biosynthesis of poly-*N*-acetyllactosamine sequences. In contrast, there were multiple genes whose transcription was upregulated in this region: two *N*-acetylglucosaminyltransferases (B3GNT-3, -8, related to the elongation of branched *N*-glycans), two *N*-acetylgalactosyltransferases (GALNT-9, -14, involved in the formation of *O*-glycan core structures) and GCNT3, also involved in *O*-glycosylation (**Figure 6).** The expression of a sialidase (NEU2) is also significantly increased (by 11.51-fold).

In the case of the striatum, in the ILBD group there is a significant upregulation in mannosidases expression (3.14-fold and 4.00-fold increase in MAN2A-1, -2, respectively, which are

the final players in the *N*-glycans maturation pathway, controlling the conversion of the oligomannose structures to complex ones), and enzymes involved in *O*-glycosylation (C1GALT1, GALNT9, GCNT3, POMGNT1) (**Figure 6).** It is also important to mention the significant upregulation of NAGPA (3.52-fold) and B3GNT-2, -8, seen both in the ILBD and PD striatum, which might indicate that the changes in these pathways start from the early stages of the disease. The expression of protein kinase C substrate 80K (PRKCSH) transcript is significantly increased as well in ILBD. This is a crucial enzyme for the formation of *N*-glycans since it cleaves glucose residues from the LLO formed in the *N*-glycans synthesis. Interestingly, multiple enzymes responsible for regulating the initial stages of the *N*-glycans formation are upregulated in the ILBD group. This might suggest that an adaptive response from the cellular machinery is taking place to compensate for the initial toxicity seen with the formation of the Lewy bodies. However, it is worth keeping in mind that the expression of the genes does not entirely reflect the expression of the final form of the enzymes. Also, their activity might be affected due to the pathophysiological conditions of the cellular milieu.

To assess the expression of the enzymes whose transcripts were evaluated previously, the proteomic profile was assessed by nanoLC-MS. Unfortunately, the expression of the glyco-enzymes of interest is low, so only very few of them were detected (**Figure 6**).

Increase in specific ER stress markers is seen in the Substantia Nigra of PD brains

Since the ER plays a pivotal role in regulating protein homeostasis and is closely related to *N*-glycosylation, UPR was also assessed through the expression of different markers using western blot.

There were no significant changes in the markers assessed in the striatum, apart from the expression of PDI, which was significantly downregulated upon PD (31.3% reduction) (**Figure 7**). In the case of the substantia nigra, there was a significant increase in the expression of partial ATF6 (2.38-fold increase) and PDI (1.51-fold increase)-classic markers of UPR activation (**Figure 7**).

The expression of other chaperones (GRP78, GRP94) was not significantly altered upon disease in either of the regions studied using western blot. However, when the proteomic analysis was

performed using nanoLC-MS, an upregulation was found in these chaperones and PDI in the substantia nigra, indicating an overall upregulation in this canonical pathway (**Figure 7)**. The undetected changes seen through western blot can be due to the defective binding between the antibody and the antigen present in each of these proteins.

DISCUSSION

The focus of this study was to characterise the protein glycosylation profile upon disease by studying the changes in the different *N*-glycosylation traits, which complements the "glyco-" studies already published on the dysregulation of GAGs[17] and the *O*-glycome[18] in human brain PD samples. *N*-glycosylation traits were analysed in parallel and correlated with the alterations seen in the transcriptomics and proteomic expression of *glyco*-enzymes and the UPR in the two regions studied and in the two diseased stages (ILBD and PD Braak stages 3/4).

The overall high abundance of fucosylated and oligomannosylated structures seen through the lectin array corroborates what was reported previously[21,22]. This array also showed the presence of GalNAc-containing *O*-glycans, being in accordance with the study exploring the *O*-glycome of PD brains[18]. Some significant changes were seen in the substantia nigra, where a decrease in the expression of lectins binding to mannose, galactose and GlcNAc was detected upon PD. However, it is worth noting that lectins have a broad range of ligands, so they can be used to detect carbohydrates in both glycoproteins and glycolipids, failing to show any distinction in the nature of the glycosylated molecule[23]. Because the focus of this study was to elucidate specifically the *N*-glycome of the human brain, further analyses were performed using an optimised multi-faceted approach combining liquid chromatography, exoglycosidase digestions and mass spectrometry, which allowed elucidation of the in-depth composition of the nigrostriatal *N*-glycoprofile, and then investigation of the alterations in each glycosylation trait upon disease.

An overall low degree of sialylation seen (around 20%) accords with previous studies reporting the *N*-glycome from other human brain regions[21] and a study on the *N*-glyco profile of the nigrostriatal pathway in the rat[24]. The increase in sialic acid seen in the *N*-glycans from both regions upon PD occurs in parallel with the increase in sialylation in the *O*-glycans from the same regions[18]. This is in contrast to studies on the *N*-glycome profiling of IgG from PD patients where sialylation is reduced[25]. Increases in sialylation have been associated with brain tumours[26] to escape from immune checkpoints, which suggests that there are proteins constituents of Lewy Bodies that are

oversialylated, preventing their elimination. However, such hypothesis will need to be further studied. A decrease in sialylation has been associated with neuroinflammatory models, mainly through the upregulation of neuraminidase 1 and 4 (NEU1 and NEU4), which constitute an essential factor for pathophysiological consequences upon inflammation[4,27]. Similar changes in the expression of neuraminidases are described in this study as an increase in the expression of NEU2 and NEU4 transcripts in the striatum upon disease is seen. However, the overall sialylation is increased, raising the question as to whether this is due to the action of sialyltransferases or to impairments in the lysosomal degradation of such proteins[28].

On the other hand, in the substantia nigra the expression of NANS was significantly upregulated, indicating a higher abundance in sialic acid substrates upon PD. Additionally, the downregulation of NEU1 and NEU2 transcripts upon PD is involved with the overall increase of sialylation. However, such conclusions will require further analysis of these enzymes' expression since they were not detected through proteomics.

Polysialic acids (PSA) are mainly seen in the neural cell-adhesion molecule (NCAM). These are known to be involved in synaptic plasticity in brain development and were reported to be upregulated in the hippocampal regions of AD patients with neuronal loss and aggregation of amyloid plaques[29]. The decrease seen in the PSA expression in the substantia nigra is parallel to decreased expression of the sialyltransferases ST8SIA3, ST8SIA4 and ST8SIA6 transcripts, suggesting the role of these sialyltransferases on the assembly of PSA.

Oligomannose structures are usually transient biosynthetic structures of *N*-linked glycans that in the case of the CNS are transported to the cell membrane to integrate the cellular glycocalyx as part of recognition molecules like NCAM or an adhesion molecule on glia (AMOG)[5]. In the adult brain, these are mainly present at the synapses, being the extent and quality of mannosylation regulated with synaptic maturation. Additionally, expression of mannose-binding lectins (MBL) has been reported in the brain, predominantly in astrocytes and microglia which are chief participants in controlling immune responses[30] through the lectin pathway of complement activation. An increase

in mannose structures abundance suggests an increased binding to these receptors, which leads to immune cell activation and inflammatory response. PD is associated with a chronic state of inflammation and reports have shown that the expression of cytokines varies between striatum and substantia nigra, amongst healthy and ILBD and PD patients[30], enhancing the inflammatory pathology. This is further confirmed by the high expression of Iba1+ and changes in microglial morphology in our study. Additionally, since these structures are abundantly present at the synapsis, and synaptic disruption was recently reported in the PD substantia nigra through PET imaging of synaptic vessel glycoprotein[31], one can hypothesise that these oligomannose residues-carrying proteins are incorrectly released to the extracellular space, that are recognised as foreign and binding to the MBL, which activates the complement system.

In the case of the striatum, it seems that the decrease in mannose expression accompanies the decrease in dopamine. It has been shown that dopaminergic agonists that act on adenylate cyclase-linked dopamine receptor sites induce a dose-dependent enhancement in the incorporation of mannose into glycoproteins in *ex vivo* models of rodent striatal cultures[32], so it can be hypothesised that a reversed effect is seen due to the depletion of dopamine in this brain region. Moreover, there is a significant increase in the expression of some mannosidases, which can trim the oligomannose structures and reduce their abundance in the diseased group. Interestingly, this relatively reduced abundance of oligomannose structures was also reported in the free IgG in the serum of PD patients[25,30].

Concerning fucosylation, its importance in *N*-glycans in the CNS requires further study. Fucose residues can be added to the glycan structures by the activity of one or more of the thirteen fucosyltransferases reported in the human genome; however, only nine are involved in the formation of *N*-glycan structures[33]. None of these enzymes was detected through proteomic analysis, nor were their transcripts differently regulated, so it was impossible to conclude if their activity was involved with the detected changes in fucosylation.

Models that fail to express core fucosylation (FUT8-knock out) show an impairment in hippocampal long-term potentiation, presenting a schizophrenia-like behaviour and phenotype[34]. This is accompanied by a significant increase in the abundance of microglia and astrocytes and their susceptibility to pro-inflammatory compounds, reaffirming that these phenotypes are due to defective neuronal physiology and dysfunctional glia populations[35]. Considering this, a decrease in core fucosylation in the PD brain would be expected. But conversely in this study, an upregulation was seen. This is likely a contradiction in the understanding of the neurodegeneration pathway of PD that mediates pathfinding for neurons or direct neurite migration[33]. However, this hypothesis will have to be further assessed.

The function of outer arm fucosylation has not been completely understood. Still, the increase seen in this trait seems to be related to the increase in *N*-glycan complexity at the later stages of the disease in the striatum.

As for galactose residues, these act as anchors for sialic acids, which are particularly important in the healthy brain, where sialylated *N*-glycans with multiple β1,3-linked galactoses and repeating units of PolyLac and a terminal galactose are abundant[36]. Also, galactose residues that belong to *N*-acetyllactosamine moieties are recognised by galectins (e.g. galectin-1, -3, -9), which have reportedly been expressed by activated microglia and astrocytes, and are involved in neuromodulation in CNS pathophysiology, mainly by controlling inflammatory processes[37]. Therefore, the increase in galactosylation seen was expected. Proteomic analysis showed a slight upregulation in galectin-1 expression in the substantia nigra but no changes were seen in the striatum.

The abundance of branched *N*-glycans is low; however, they are an essential posttranslational modification for neuronal survival since the knock-down of *N*-acetylglucosaminyltransferase 1 (MGAT1; enzyme responsible for initiating the formation of hybrid glycans) leads to apoptosis and severe behaviour impairments, tremors and premature death[38]. The abundance of bisecting and branched *N*-glycans is intimately connected since both involve adding GlcNAc residues by *N*-acetylglucosaminyltransferases (MGAT) to a mannose donor, and the existence of bisecting GlcNAc

can limit the synthesis of branched structures. The presence of the bisecting GlcNAc (mediated by MGAT3) inhibits the action of other glycosyltransferases (mainly MGAT4, MGAT5)[39].

The expression of MGAT3 was described to increase in the AD human brain, reflecting an adaptive response to protect the brain as this increase occurs post-accumulation of β–amyloid and reduces Aβ production to protect against neurological degeneration[39]. Even though the expression of Beta-1,4-mannosyl-glycoprotein 4-beta-*N*-acetylglucosaminyltransferase (MGAT3) transcript was not altered in PD brains, it is possible that the expression and/or activity of the enzyme is altered, so the increase in bisected glycans seen in the striatum can be perceived as being adaptive and protective.

The dysregulation of certain *N*-glycan structures was also reported through MALDI-MSI in AD brains[40]. A region-specific modulation of *N*-glycans upon disease was also seen in this case. For example, FA2G1 (1647 m/z), FA2G2 (1809 m/z) and FA3G1 (1850 m/z) were all shown to be decreased upon AD in the hippocampus, but increased in the cortex from the diseased brains[40]. Interestingly, FMA5A1 (1606 m/z, decreased in the PD striatum) was also decreased in the hippocampus of the AD brains. On the other hand, FA2F1G1 and FA3F1G1 (1793 m/z and 1996 m/z, respectively) were both increased in the cortex of AD brains, whereas they were downregulated in the striatum and substantia nigra (respectively) of PD brains. This indicates that these might be specific to each condition and potentially play different roles on the onset of distinct neurodegenerative diseases, also depending on the brain region where they are expressed.

Concerning the interplay between ER stress and changes in *N*-glycosylation, it has been reported that the increase in spliced X-box binding protein 1 (XBP1) due to the activation of the IRE-1 branch of the UPR leads to a decrease in bisecting glycans and sialylation and increases oligomannose structures[41], which corresponds to the nigral PD *N*-glycomic signature. Here we saw changes in the ATF6 branch of the UPR and in other markers in the substantia nigra, which indicate that the UPR plays a role in the alterations seen in the *N*-glycomic profile since polysialylation and bisects decreased significantly and mannosylation increased in this region.

It is in the ER that *N*-glycosylation begins[12] and where glycan structures are further trimmed by resident glucosidases and mannosidases, and directed either for proper protein folding, exportation or ERAD[10]. Even though most *glyco*-enzymes act on the Golgi apparatus, the cell machinery relies on the activity and physiological conditions of the different organelles, which emphasises the importance of looking at ER stress/UPR in the context of an *N*-glycosylation-based study.

It was shown that ER stress is linked with dopaminergic neuronal death as different markers were shown to be significantly upregulated post-stimuli with toxins such as 6-OHDA or MPP+, both *in vitro*[42] and *in vivo*[43]. Also, UPR activation was correlated with the aggregation of α-syn in human samples[44]. Nonetheless, most of these studies cover only a few of the players involved in UPR. Therefore, it is essential to look at the overall picture and assess the different cascades of the UPR response, mainly the ATF6 pathway, which hitherto has been overlooked.

Only some of the markers were differently regulated through western blot (PDI and ATF6) in this study. However, this analysis was further complemented by proteomic analysis, where an upregulation of chaperones was seen (BiP and GRP94). The main function of PDI is to catalyse the formation and rearrangement of disulphide bonds in molecules (essential for proper protein folding). It has been reported that PDI has anti-inflammatory properties, inhibiting the LPS produced by macrophages[45]. Therefore, the increase in the expression of PDI seen in the substantia nigra is in line with the inflammatory profile seen and confirms an increase in UPR. Since there is also the accumulation of aggregated α-syn in these samples (demographic data supplied by Parkinson's UK Brain Bank), it confirms the link between UPR and protein aggregation[44].

The upregulation in the expression of the cleaved ATF6 in the substantia nigra also indicates the activation of another branch of the UPR. Cleavage of ATF6 was not detected through proteomics, so western blot was the best approach to assess this. This cleavage also leads to the upregulation of PDI, which explains the increase in both of these markers seen in the substantia nigra of PD patients[46]. In a rodent model of PD (MPP+) it was shown that ATF6 was significantly increased post

injury, and that animals deficient in ATF6 displayed increased loss of dopaminergic neurons[47]. It is, possible, therefore, that the changes seen in the different situations relate to the dynamic and flexible nature of the UPR and/or to the techniques used to quantify these changes. In either case, it is essential to explore the different cascades and players involved in the UPR.

To sum up, this study presents for the first time a comprehensive overview of the different "omic" branches of PD that relate to *N*-glycosylation in a region-dependent manner, providing information on how they interplay with disease progression, exploring pathways that were previously overlooked (**Figure 8**). While it is naive to assume that these dysregulations are directly correlated, it is still a valid starting point that was not considered to date. Having this overview of how the *N*-glycome is altered in parallel with the other pieces of the PD molecular signature such as the expression of *glyco*-enzymes, the UPR and the proteomic profile can help to preliminarily establish a pattern in a non-template-driven process. Further studies on how ER stress in the dopaminergic circuitry might be leading to *N*-glycosylation dysregulation will be of utmost interest.

METHODS

Human brain tissue

Frozen autopsied striatum and substantia nigra from patients with Parkinson's Disease (n=12 (snap frozen tissue), n=6 (fixed-frozen, 10µm thick sections)) or Incidental Lewy Bodies Disease (n=3 (snap frozen tissue), n=1 (fixed-frozen, 10µm thick sections)), healthy matched controls (n=15 (snap frozen tissue), n=6 (fixed-frozen, 10µm thick sections)), and associated clinical and neuropathological data were supplied by the Parkinson's UK Brain Bank, funded by Parkinson's UK, a charity registered in England and Wales (258197) and in Scotland (SC037554). The gender, age, post-mortem delay, duration of the disease and Braak stages are described in **Table S2**. All experiments were done in accordance with the NUI Galway Research Ethic Committee guidelines, under the reference of 18-Mar-20.

Tissue homogenisation

The snap frozen brain tissue was homogenised in different ways depending on the assay performed. For the glycomic analysis, the snap frozen brain tissue was homogenised in RIPA® buffer (R0278, Sigma, Ireland) and cOmplete™ Protease Inhibitor Cocktail (5056489001, Roche, Ireland, 1:25) through mechanical disruption using Qiagen TissueLyser LT (Qiagen, UK), at 4ºC (40Hz, 8 minutes). The homogenates were centrifuged at 16.000 g for 20 minutes at 4ºC and the supernatants were collected for further analysis. The protein concentration of the supernatants was calculated using the Pierce™ BCA Protein assay kit (23225, Thermo-Fisher, UK). For the proteomic analysis, tissue was lysed in 100mM Tris (pH 8.5) with 1% sodium deoxycholate, 10 mM TCEP, 40 mM chloroacetamide and cOmplete™ Protease Inhibitor Cocktail. The samples were vortexed, boiled for 5 minutes and sonicated on ice. The homogenates were centrifuged at 20.000 g for ten minutes and the supernatants were collected for further analysis.

Lectin microarray

Microarray fabrication

Lectin solutions (0.4 - 0.5 mg/mL) and antibody solutions (0.1 mg/mL) were prepared in buffer (1.0mM D-glucose in PBS containing 0.01% of cy3-conjugated BSA). 0.67 nL of these dilutions was printed onto NHS functionalised glass slide. The slides containing the lectin arrays were incubated after printing in a 75% humidity chamber at 18ºC overnight. The remaining NHS groups were quenched by placing the slides in a 30mM ethanolamine solution in borate buffer and then blocked with a 0.3 mg/mL BSA,

0.3mM Ca^{2+} solution in PBS-T 0.05%. The slides were directly dried by centrifugation without previously washing. All the lectins used in the microarray are listed in **Table S3**.

Sample buffer change

To prevent possible interference from the sample buffer (RIPA® buffer (R0278, Sigma, Ireland) and cOmplete™ Protease Inhibitor Cocktail (5056489001, Roche, Ireland)), during the labelling step the buffer was changed using 0.5mL 10kDa Amicon™ spin filters (Merck, Ireland). 30 µg of each sample was added to the spin filter and washed twice with PBS by centrifugation (Beckman Coulter Allegra X-22R Centrifuge). Glycoproteins were recovered at a final concentration of 0.3 µg/µL in PBS.

Sample labelling of glycoproteins

10 µL of PBS 10x (500 mM, pH=8.3) was added to the 0.3 µg/µL solution of glycoprotein in PBS prepared previously (100µL). Afterwards, the solution was incubated with 0.45 µL of Alexa-555-NHS dye (10 µg/µL in DMSO) for 1h at room temperature. The excess dye was quenched by the addition of Tris buffer and the fluorescently labelled glycoprotein solutions were directly used in the lectin array analysis.

Incubation of lectin array

The glycoprotein samples (at a concentration of 3 µg/mL) were added to the corresponding wells (previously printed on the slides) and incubated for 1h 30 at room temperature. The sample concentration was adjusted by adding lectin incubation buffer to the labelled glycoprotein solutions after labelling. Labelled-BSA and control dye samples were incubated under the same conditions as negative controls for lectin binding. Then the glycoprotein solutions were removed and the slide washed with PBS, dried by centrifugation and scanned on a G265BA microarray scanner (Agilent Technologies).

Microarray data interpretation and statistical analysis

The images obtained were analysed with Pro Scan Array Express® software (PerkinElmer). Two-way ANOVA was performed, followed by Tukey's post-hoc test and statistical significance set at $*p<0.05$ and $**p<0.01$.

Dual lectin and immunohistochemistry

Frozen tissue sections (10 µm thick) were warmed at room temperature for at least 45 minutes before beginning the staining. Sections were washed with 0.05% Triton-X (TBS-T) in Tris-buffered saline supplemented with Ca^{2+} and Mg^{2+} (TBS: 20 mM Tris-HCl, 100 mM NaCl, 1 mM $CaCl_2$, 1 mM $MgCl_2$, pH 7.2) three times during three minutes with gentle shaking. Then these sections were blocked with 3% periodate-treated high grade bovine serum albumin (pBSA) made in TBS for one hour at room temperature to block unspecific binding[23,48]. The sections were then washed again three times with TBS for three minutes each wash. Afterwards, they were incubated with fluorescently labelled lectins (**Table S4**) prepared in TBS-T for one hour in the dark at room temperature. After washing the sections again with TBS, these were blocked again with 3% pBSA for one hour at room temperature and then incubated with primary antibodies (anti-glial fibrillary acid protein (GFAP) produced in rabbit (Dako, USA, Z0334, 1:400) or anti-Ionized calcium binding adaptor molecule 1 (Iba1) produced in rabbit (Wako, USA, 019-1941, 1:500)) overnight at 4°C. After 24h, sections were washed in TBS-T and TBS and incubated with the secondary antibody at room temperature for one hour (AlexaFluor 594 goat anti-rabbit IgG (H+L) (Invitrogen, Ireland, A-11012, 1:1000) in TBS. These were then washed with TBS-T and TBS and finally counterstained with Hoechst (ThermoFisher, Ireland, 33342, 1:2000 in TBS) for 15 minutes. Subsequently the sections were washed again in TBS and incubated with 0.2% sudan black B solution (since this is effective in quenching the autofluorescence from lipofuscin, a substance consisting of oxidised lipids and common in aged brains) in 70% ethanol to quench lipofuscin auto fluorescence (granules that accumulate with age in the human brain). After washing twice with TBS, sections were mounted using fluoromount aqueous mounting medium (Sigma, Ireland, F4680) and coverslips and imaged within three days after curing. Inhibition by the appropriate haptenic sugar was used as control for all lectins in the study.

DMB assay

Release of sialic acids

To assess the type of sialic acids present in the brain glycoproteins, a kit was used to release the sialic acids and label them with 1,2-diamino-4,5-methylenedioxybenzene Dihydrochloride (DMB). After homogenising the tissue as described previously, the glycoprotein solution was dried in a SpeedVac (Savant™ SPD131DDA SpeedVac™ Concentrator, ThermoFisher) overnight. On the next morning, 25 µL of 2M acetic acid solution was added to each sample, to the controls and the standards. These were briefly vortexed and centrifuged. Then they were incubated at 80°C for two hours and cooled to room temperature afterwards. 5 µL from each vial was kept at -20°C for the following steps.

DMB labelling

For the sample labelling, 440µL of the mercaptoethanol solution was added to the vial of sodium dithionite and mixed until dissolved. This solution was then added to the DMB dye and mixed. Afterwards, 20µL of this labelling reagent was added to each sample, controls and standards, mixed thoroughly and briefly centrifuged. Then the vials were incubated for three hours at 50°C in the dark. The reaction was terminated by the addition of 475 µL of water to each sample and control or of 480 µL of water to each sialic acid standard.

Ultra-high performance liquid chromatography (UHPLC)

UHPLC was performed to analyse these samples using the LudgerSep™ uR2 UHPLC column, 175 A, 1.9 µm silica derivatised particles with octadecylsiliane coating, 2.1 x 100mm (Luger, UK) on an Acquity system. Solvent A was acetonitrile:methanol:water (9:7:84) and solvent B was acetonitrile. The sample temperature was set to 10°C and the column temperature to 30°C. The method had a 15 minute duration, the flow rate was constant at 0.25 mL/min. During the first 7 minutes, the flow was solely composed of solvent A. This was reduced to 10 % (and solvent B increased to 90%) between 7.5 and 8 minutes, and returned to the initial values between minute 8.5 and 15.

N-acetylneuraminic acid quantitative standard, *N*-glycolylneuraminic acid quantitative standard and a sialic acid reference panel containing Neu5Ac, Neu5Gc, Neu5,7Ac2, Neu5Gc,9Ac, Neu5,8Ac2, Neu5,9Ac2 and Neu5,x,xAc3 (where x is an unknown acetyl position) were used at the beginning of the run to calibrate the system. All of these were included in the kit. A negative control with only buffer (without sample) was also used.

N-glycan analysis

Isolation and fluorescence labelling of N-glycans

The isolated glycoproteins were dried in a vacuum centrifuge overnight (Savant™ SPD131DDA SpeedVac™ Concentrator, ThermoFisher). These were immobilized in an acrylamide gel and reduced and alkylated. *N*-glycans were released using *N*-glycanase PNGase F (1239U/ml, New England BioLabs, Inc. cat no. P0709L) and were fluorescently labelled with 2-aminobenzamide (2-AB) by reductive amination[24,49,50], and the excess of 2-AB was removed on Whatman™ 3MM paper (Clifton, NJ) in acetonitrile washes[51].

Hydrophilic interaction liquid chromatography – ultra performance liquid chromatography (HILIC-UPLC)

UPLC was performed using a UPLC Glycan BEH Amide Column, 130A, 1.7 µm particles, 2.1 x 150mm (Waters, Milford, MA) on an H Class Acquity™ UPLC (Waters, Milford, MA) equipped with a Waters temperature control module and a Waters Acquity™ fluorescence detector. Solvent A was 50 mM ammonium formate, pH4.4 and Solvent B was acetonitrile. The column temperature was set to 40°C and the sample temperature to 5°C. The method had a duration of 30 minutes and it was composed of a linear gradient of 30% to 47% of buffer A for 24 minutes at 0.561mL/min flow rate, increasing to 70% at minute 25 and returning to 30% at minute 27 until the end of the run. Samples were injected in 70% acetonitrile. Samples were excited at 330 nm and fluorescence was measured at 420. nm. For each sample set, the system was calibrated using a dextran ladder of 2AB-labelled glucose oligomers (Waters, Milford, MA), as described elsewhere[50].

Weak anion exchange – ultra performance liquid chromatography (WAX-UPLC)

WAX-UPLC was carried out using a DEAE anion exchange column, 10 µm particle size, 75 x 7.5mm on a Water Acquity™ UPLC separations module complete with a Waters Acquity™ UPLC fluorescence detector. Solvent A consisted of 20% v/v acetonitrile in water and solvent B was 0.1M ammonium acetate buffer, pH7.0, in 20% v/v acetonitrile. This method had a duration of 30 minutes and the gradient conditions were a linear gradient of solvent A from minute 5 to minute 20 from 100% to 0%. At minute 23 solvent A returns to 100%, remaining constant until the end of the run, all at a 0.750 mL/min flow rate. Samples were injected into water. Samples were excited at 330 nm and fluorescence was measured at 420 nm. For each sample set, the system was calibrated using *N*-glycan extracted from fetuin[50].

Glycan nomenclature

All *N*-glycans share the same pentasaccharide core composed of two core GlcNAcs linked to three mannoses. F at the start of the abbreviation indicates a core α(1,6)-fucose linked to the inner GlcNAc. Otherwise, F indicates an outer arm α(1,3) or α(1,4)-fucose linked to antenna or galactose. Mx indicates the number (x) of mannose residues on the core GlcNAcs. Ax refers to the number (x) of GlcNAc (antenna) on the trimannosyl core. Gx relates to the number (x) of β(1,4)-linked galactose on the antenna and Galx to the number (x) of α(1,3/4/6)-linked galactose on β(1,4)-linked galactose. Sx stands for the number (x) of sialic acids (neuraminic acids) linked to galactose, through an α(2,3)-, α(2,6)- or α(2,8)-linkage depending on the number inside the parentheses (3, 6 or 8, respectively). Sgx concerns the number (x) of glycolylneuraminic acids linked to galactose, and the number in

parentheses corresponds to the linkage as before. Lacx indicates the number (x) of poly-*N*-Acetyllactosamine repeats containing GlcNAc linked β(1,4)- to galactose.

Exoglycosidase digestions of 2-AB labelled N-linked glycans

The 2-AB labelled *N*-glycans were digested in a volume of 10 µL for 18h at 37°C in 50 mM sodium acetate buffer, pH5.5 (except jack bean α-mannosidase (JBM), which was in 100 mM sodium acetate, 2 mM Zn^{2+}, pH 5.0). The enzymes used were: *Arthrobacter urefaciens* sialidase (ABS), 0.5U/mL; *Streptococcus pneumoniae* sialidase (NAN1), 5U/mL; bovine testes β-galactosidase (BTG), 1U/mL; bovine kidney α -fucosidase (BKF), 1U/mL; almond meal α-fucosidase (AMF), 400U/mL; β-N-acetylglucosaminidase cloned from *Streptococcus pneumonia* (GUH), 400U/mL; JBM, 400U/mL; *Streptococcus pneumoniae* β-galactosidase (SPG), 0.4U/mL; coffee bean α-galactosidase (CBG), 25U/mL. Enzymes were purchased from Prozyme (San Leandro, CA, USA) (ABS, NAN1, BTG, SPG, CBG, BKF, JBH) or New England Biolabs (Hitchin, Herts, UK) (AMF, JBM, GUH). After incubation, enzymes were removed by filtration through 10kDa MWCO microcentrifuge filtration tubes (Pall Corporation, NY, USA). Digested *N*-glycans from the different samples were analysed by HILIC-UPLC[50].

Liquid chromatography-mass spectrometry (LC-MS)

For liquid chromatography fluorescence quadrupole time-of-flight mass spectrometry (UPLC-FLR-QTOF MS) analysis, the dried *N*-glycan samples were reconstituted in 3 µL of milliQ water and 9 µL acetonitrile. Online coupled fluorescence (FLR)-mass spectrometry detection was performed using a Waters Xevo G2 QTof with Acquity™ UPLC (Waters Corporation, Milford, MA, USA) and BEH Glycan column (1.0 x 150mm, 1.7 µm particle size). Sample injection volume was 10 µL. The flow rate was 0.150 mL/min and column temperature was kept at 60°C. Solvent A was 50 mM ammonium formate (pH 4.4) and solvent B was acetonitrile. A 40 minute linear gradient was used and was as follows: Solvent A at 28% for one minute, increase from 28% to 43% for 30 minutes, increase from 43% to70% for one minute, constant at 70 % for three minutes, decrease from 70% to 28% for one minute and constant at 28% for four minutes. To avoid contamination of the system, the flow was sent to waste for the first 1.2 minutes and after 32 minutes. The fluorescence detector settings were as follows: λexcitation: 320 nm, λemission: 420 nm; data rate was 1 pts/second and a PMT gain = 10.

For mass spectrometry (MS) acquisition data, the instrument was operated in negative-sensitivity mode with a capillary voltage of 1.8 kV. The ion source block temperature was set at 120°C and the nitrogen desolvation gas temperature was set at 400°C. The desolvation gas had a flow rate of 600 L/h. The cone voltage was kept at 50 V. Full-scan data for glycans were acquired over m/z range

of 450 to 2500. Data was collected and processed using MassLynx™ 4.1 software (Waters Corporation, Milford, MA, USA).

Matrix-assisted laser desorption/ionisation mass spectrometry imaging (MALDI-MSI) of *N*-glycans

Sample preparation

For spatial *N*-glycome analysis through MALDI mass spectrometry imaging, samples were prepared as previously described[52]. Briefly, frozen 10 µm brain tissue sections on SuperFrost™ Plus Adhesion charged slides (Fischer Scientific, Ireland) were thawed and dehydrated in serial dilutions of ethanol (70%, 90%, 100%, 100%) for two minutes each. Then, sections were incubated at 60 °C for 50 minutes, followed by delipidation in Carnoy's solution twice (30% chloroform, 10% glacial acetic acid, 60% ethanol), for three minutes, and a wash in running tap water. Finally, these were incubated with 10% formalin solution neutral buffered (Sigma, Ireland) (30 minutes), followed by two washes in tap water. The samples were then air-dried and kept in a desiccator until further analysis.

Antigen retrieval

The transformed slides were exposed to antigen retrieval using citraconic anhydride buffer (pH3), prepared by mixing 25 µL of citraconic anhydride (Sigma, Germany) in 50 mL of HPLC grade water. Slides were incubated in this buffer in a vegetable steamer (approximately 95 °C) for 30 minutes and then washed in serial dilutions of the buffer by replacing half of the buffer with HPLC grade water (three times), eventually switching it completely with water. The slides were air-dried and scanned before applying PNGase F.

Application of PNGase F and matrix

After antigen retrieval, slides were coated with an aqueous solution of recombinant PNGaseF (Serva, Germany) at 0.1 µg/ µL at 45 °C, using an HTX TM-Sprayer™ (HTX Imaging, USA) as previously described [53]. This was followed by an incubation of two hours at 37 °C in a humidified chamber and placed in the desiccator until sprayed with matrix on the same day. α-Cyano-4-hydroxycinnamic acid (CHCA) matrix was prepared fresh (7 mg/mL in 50% acetonitrile 0.1% TFA) and applied in the sections at 100 µL/ min at 79 °C using an HTX TM-Sprayer™. Coated slides were stored in a desiccator until being analysed (no longer than 48 h post-spraying).

MALDI-MSI set up

Released *N*-glycan ions were detected using a MALDI FT-ICR scimaX™ (Bruker Daltonics, Germany) operating in positive mode with a Smart Beam II laser operating at 1000 Hz and a laser spot size of 20 µm. Signal was collected at a raster width of 150 µm between spots. A total of 300 laser shots was collected to form each pixel. Following the acquisition, data was processed and images of expressed glycans were generated using FlexImaging™ 5.0 and SCiLS™ Lab 2021 software (Bruker Daltonics, Germany), where ions in the range of 900-3200 m/z were analysed. Observed mass/charge ratios (*N*-glycans) were searched against the glycans assigned and detected through LC-MS previously, glycan databases using GlycoWorkbench® and the database provided by the Consortium for Functional Glycomics (www.functionalglycomics.org). Represented glycan structures were also generated in GlycoWorkbench®, as they were determined by a combination of their measured accurate m/z, CID fragmentation patterns and previous structural characterisation carried out by HILIC-UPLC.

Gene array

mRNA extraction

Brain tissue from the striatum and substantia nigra was homogenized and lysed in TRI Reagent® (Sigma, Ireland). The insoluble material was removed by centrifugation, from which only the supernatant was collected. To this, 1-Bromo-3-chloropropane (BCP) was added and mixed. Afterwards, this was centrifuged and the aqueous phase collected as it contained the mRNA. Finally, isopropanol was added to precipitate the nucleic acids, and these were washed in a gradient of ethanol solutions, being stored in THE RNA storage solution® (Invitrogen, Ireland, AM7000). The concentration, purity and integrity of the RNA were checked using the NanoDrop™ 2000c Spectrophotometer (Thermo Scientific, UK) (reading at 260/230 nm and 260/280 nm of wave length), and the BioAnalyzer™ 2100 (Agilent, USA).

cDNA reverse transcriptase

cDNA synthesis was performed using the RT^2 first strand kit (Qiagen, UK) and following the manufacturer's instructions. Briefly, initially the genomic DNA was eliminated using a starting amount of 450 ng of mRNA and the buffer GE present in the kit, warming it for 5 minutes at 42^{o}C. This was followed by incubation with the reverse transcription mix (as described by the manufacturer), for 15 minutes at 42^{o}C and then for 5 minutes at 95^{o}C. The cDNA was stored at -20^{o}C until further use.

Glycosylation gene array

cDNA was labelled with SyBR Green using an RT^2 SyBR Green Mastermix provided by the manufacturer, which contained a HotStartDNA® *Taq* Polymerase (Qiagen, UK). This mixture (containing the labelled cDNA) was dispensed into the 384-wells of each plate (10 uL per well) containing 86 primers for the genes encoding for glycosylation genes such as glycosidases and glycosyltransferases (**Table S5**). The plate was inserted in the Roche LightCycler® 480 (Roche Life Science, Switzerland) and the cycles were defined as follows: 1 cycle for ten minutes at 95°C, and 45 cycles of 15 seconds at 95°C and one minute at 60°C. The data acquired was analysed using the GeneGlobe Data Analysis Centre® (Qiagen, UK). Significant upregulation or downregulation of the different genes was considered when fold change ≥ 3 and $p \leq 0.05$. The collected data represents the pool of mRNA from six biological replicates for the healthy group, three for the ILBD group and six for the PD group.

Western blot

Protein lysates from brain samples previously homogenised in RIPA buffer (R0278, Sigma, Ireland) and cOmplete™ Protease Inhibitor Cocktail (5056489001, Roche, Ireland, 1:25) were boiled at 95°C for seven minutes with loading buffer containing 1% bromophenol blue and 200mM of DTT. Equal amounts (5 µg or 10 µg, depending on the detection antibody) of protein samples were run on an SDS polyacrylamide gel with 12% or 15% acrylamide depending on the size of the proteins to be detected. After the run, the proteins were transferred onto a 0.45 NC nitrocellulose membrane (Fisher Scientific, Ireland) using the Trans-Blot® Turbo™ transfer system (Biorad, UK). Ponceau red S staining was performed to confirm the presence of the proteins in the membrane. The ponceau red was washed off with 5% acetic acid and then the membrane was washed with TBS-T (tris buffered solution with 0.05% Tween20). The membrane was blocked with 5% milk in TBS-T for one hour at room temperature. This was followed by incubation with primary antibody for GRP94 (Cell Signalling Technology, The Netherlands, 2104S, 1:1000), PDI (Cell Signalling Technology, The Netherlands, 3501S, 1:1000), GRP78 (Abcam, UK, ab32618, 1:3000), ATF6 (Abcam, UK, ab37149, 1:750), phospho-eIF2α (Cell Signalling Technology, The Netherlands, 9721S, 1:1000), ATF4 (Cell Signalling Technology, The Netherlands, 11815S, 1:1000) and CHOP (Cell Signalling Technology, The Netherlands, 2895S, 1:1000) overnight at 4°C. On the next day, the membrane was washed three times with TBS-T and incubated with the appropriate horseradish peroxidase-conjugated secondary antibody (Goat anti-mouse IgG, Fisher Scientific, Ireland, 31430, 1:10000, or goat anti-rabbit IgG, Fisher Scientific, Ireland, 31460, 1:10000) for one hour at room temperature. After three washes in TBS-T, signals were detected using SuperSignal™ WestPico PLUS ECL (Fisher Scientific, Ireland, 34577). Quantification of the signal

intensity was performed using Image Studio Lite and normalised by the expression of β-actin (which was carried out in all the blots performed). If the data was normally distributed, one-way ANOVA was performed, followed by Dunnett post-hoc test, and statistical significance was set at *p<0.05. If the data was not normally distributed, a Kruskall-Wallis test followed by a Dunn's post hoc test were carried out, and statistical significance was set at *p<0.05.

Proteomic analysis

Protease digestion

Proteins (200 µg) were digested with trypsin at an enzyme to substrate ratio of 1:50 (w/w) for 18 hours at 37 ^{o}C, and then stopped by acidification with formic acid (FA). to a final concentration of 2% (v:v). Peptides were desalted using C18 Sep-Pak cartridges following the manufacturer's instructions, dried, and the peptide concentration was determined using the Thermo Scientific™ Pierce™ Quantitative Fluorimetric Peptide Assay.

TMT-labelling

Peptides were reconstituted in 40 µL of 100 mM Triethylamonium bicarbonate (TEAB), and tandem mass tag (TMT) labelling was carried out on 30 µg of peptides from each individual sample. Samples were distributed in the 11-plex label set. TMT labelling reagents were each dissolved in 20 µL anhydrous acetonitrile. Each sample containing 30 µg of peptide in TEAB buffer was combined with 20 µL of its respective 11-plex TMT reagent and incubated for one hour at room temperature. Then, 4 µL of 5% hydroxylamine was added, and the combined sample incubated for a further 15 minutes. This mixture was then dried for further analysis.

Nano-LC mass spectrometry

The dried sample was resuspended in 5% formic acid and desalted using a SepPak® cartridge according to the manufacturer's instructions (Waters, UK). Eluate from the SepPak® cartridge was again dried and resuspended in buffer A (20 mM ammonium hydroxide, pH 10) prior to fractionation by high pH reversed-phase chromatography using an UltiMate® 3000 liquid chromatography system (Thermo Scientific).

For reversed-phase chromatography, an XBridge BEH^{TM} C18 Column (130 Å, 3.5 µm, 2.1 mm X 150 mm, Waters, UK) was used, and peptides were eluted with an increasing gradient of buffer B (20 mM Ammonium Hydroxide in acetonitrile, pH 10) from 0% to 95% over 60 minutes. The resulting fractions were dried and resuspended in 1% formic acid prior to analysis by nano-LC MSMS using an

Orbitrap Fusion Tribrid mass spectrometer (Thermo Scientific). Here, peptides in 1% (vol/vol) formic acid were injected onto an Acclaim PepMap® C18 nano-trap column (Thermo Scientific). After washing with 0.5% (vol/vol) acetonitrile 0.1% (vol/vol) formic acid, peptides were separated on a 250 mm x 75 µm Acclaim PepMap® C18 reverse phase analytical column (Thermo Scientific) over a 150 minutes organic gradient. Solvent A was 0.1% formic acid and Solvent B was aqueous 80% acetonitrile in 0.1% formic acid. Organic gradient included 7 gradient segments (1% to 6% of solvent B over one minute, 6% to 15% of solvent B over 58 minutes, 15% to 32% of solvent B over 58 minutes, 32% to 40% of solvent B over five minutes, 40% to 90% of solvent B over one minute, and then kept at 90% of solvent B for six minutes and then reduced to 1% of solvent B over one minute) with a flow rate of 300 nL/min. Peptides were ionized by nano-electrospray ionization at 2.0kV using a stainless steel emitter with an internal diameter of 30 µm (Thermo Scientific) and a capillary temperature of 275 °C. All spectra were acquired using an Orbitrap Fusion™ Tribrid™ mass spectrometer controlled by Xcalibur® 2.0 software (Thermo Scientific) and operated in data-dependent acquisition mode using an SPS-MS3 workflow.

The raw files were analysed with MaxQuant® v. 1.6.17 and searched against the latest human fasta database (version 05.2020, 20368 sequences) downloaded from UniProt. Identified peptides and proteins were filtered to 1% FDR. TMT reagent impurity correction was performed.

Data analysis: Perseus workflow and Ingenuity pathway analysis (IPA)

MaxQuant® data was exported to Perseus® software for complete proteomics analysis, where the results were log2 transformed as well as filtered to exclude any contaminants and non-significant peptides. The final data set (including the fold ratio change of each group compared to healthy and p-values) was further analysed in the Ingenuity Pathway Analysis software (IPA®, Qiagen, UK), where canonical pathways and upstream regulator data were compared by their activation z-score and associated p-value. The main proteins and pathways considered related to unfolded protein response, glyco-related proteins/enzymes and neuroinflammatory signalling.

Pathological analysis

Immunohistochemistry (chromogenic staining)

Frozen tissue sections (10 µm thick) were warmed at room temperature for at least 45 minutes before starting the staining. Sections were incubated with 0.3% hydrogen peroxidase in 70% MeOH in PBS for 20 minutes to block endogenous peroxidase. Then the sections were washed twice with PBS and blocked with 5% normal goat serum (NGS) in PBS-T (PBS with 0.2% Triton X) for one hour at room temperature. The slides were then incubated with primary antibody solution prepared in 5% NGS in PBS-T (anti-GFAP produced in rabbit (Dako, USA, Z0334, 1:400) or anti-Iba1 produced in rabbit (Wako,

USA, 019-1941, 1:500)) overnight at 4°C. On the next day the sections were washed twice with PBS and incubated with the biotinylated secondary antibody prepared in PBS for 30 minutes at room temperature. After washing twice in PBS, slides were incubated with streptavidin ABC HRP-complex (VectorLabs®, UK, PK-6100) for 30 minutes at room temperature. Then the slides were washed and incubated with 3,3'-Diaminobenzidine tetrahydrochloride hydrate (DAB) (2 mg/mL) (Sigma, Ireland, D9015) activated with 30% hydrogen peroxide for five minutes. Finally, the sections were counterstained with Heamatoxylin Gill no.2 (Sigma, Ireland, GHS216), dehydrated in ethanol, cleared in xylene and mounted with DPX mountant (Sigma, Ireland, 06522).

Haematoxylin/Eosin

Frozen tissue sections (10 µm thick) were warmed at room temperature for at least 45 minutes before the start of staining. Sections were hydrated in serial dilutions of ethanol (100%, 95%, 90%, 70%, 50% EtOH), followed by tap water. Then the sections were incubated with Heamatoxylin Gill no.2 (Sigma, Ireland, GHS216) followed by Eosin Y (Sigma, Ireland, HT110132). Finally, the slides were dehydrated in three solutions of 100% EtOH, cleared in xylene and mounted with DPX® mountant (Sigma, Ireland, 06522).

Terminal deoxynuclotidyl transferase dUTP nick end labelling (TUNEL) assay

TUNEL assay was performed using the Kit HRP-DAB from Abcam (Abcam, UK, ab206386) and the manufacturer's instructions were followed. Briefly, the frozen sections were warmed at room temperature for at least 45 minutes, permeabilised with Proteinase K (1:100) for ten minutes and washed with TBS. Sections were incubated with 3% hydrogen peroxidase in MeOH for five minutes to block endogenous peroxidase, washed with TBS, equilibrated with TdT equilibration buffer for 30 minutes and incubated with TdT labelling reaction mix in a humidified chamber at 22°C for 1h 30. The reaction was stopped with the stop buffer and the slides were washed with TBS. The sections were then blocked with blocking buffer for ten minutes at room temperature and incubated with the conjugate solution for 30 minutes at room temperature. Slides were washed with TBS and the stain developed using DAB for 15 minutes. Finally, the sections were counterstained with methyl green, dehydrated in two solutions of 100% EtOH, cleared in xylene and mounted with DPX® mountant (Sigma, Ireland, 06522).

REFERENCES

[1] W. Poewe, K. Seppi, C.M. Tanner, G.M. Halliday, P. Brundin, J. Volkmann, A.-E. Schrag, A.E. Lang, Parkinson disease., Nat. Rev. Dis. Prim. 3 (2017) 17013. doi:10.1038/nrdp.2017.13.

[2] A. Varki, R.D. Cummings, J.D. Esko, H.H. Freeze, P. Stanley, C.R. Bertozzi, G.W. Hart, M.E. Etzler, eds., Essentials of Glycobiology, Cold Spring Harbour Laboratory Press, New York, NY, 2009.

[3] R. Apweiler, H. Hermjakob, N. Sharon, On the frequency of protein glycosylation, as deduced from analysis of the SWISS-PROT database, Biochim. Biophys. Acta. 1473 (1999) 4–8. doi:10.1016/s0304-4165(99)00165-8.

[4] A.L. Rebelo, M.T. Chevalier, L. Russo, A. Pandit, Role and therapeutic implications of protein glycosylation in neuroinflammation, Trends Mol. Med. 28 (2022) 270–289. doi:10.1016/j.molmed.2022.01.004.

[5] R. Kleene, M. Schachner, Glycans and neural cell interactions, Nat. Rev. Neurosci. 5 (2004) 195–208. doi:10.1038/nrn1349.

[6] J. Jaeken, H. Carchon, Congenital disorders of glycosylation: a booming chapter of pediatrics., Curr. Opin. Pediatr. 16 (2004) 434–9. doi:10.1097/01.mop.0000133636.56790.4a.

[7] A. Helenius, M. Aebi, Intracellular functions of N-linked glycans, Science (80-.). 291 (2001) 2364–2369. doi:10.1126/science.291.5512.2364.

[8] R. Kornfeld, S. Kornfeld, Assembly of asparagine-linked oligosaccharides., Annu. Rev. Biochem. 54 (1985) 631–664. doi:10.1146/annurev.bi.54.070185.003215.

[9] R.D. Klausner, R. Sitia, Protein degradation in the endoplasmic reticulum, Cell. 62 (1990) 611–614. doi:10.1016/0092-8674(90)90104-m.

[10] Y. Yoshida, A novel role for N-glycans in the ERAD system, J. Biochem. 134 (2003) 183–190. doi:10.1093/jb/mvg128.

[11] B. Tsai, Y. Ye, T.A. Rapoport, Retro-translocation of proteins from the endoplasmic reticulum into the cytosol, Nat. Rev. Mol. Cell Biol. 3 (2002) 246–255. doi:10.1038/nrm780.

[12] M.A. Lehrman, Stimulation of N-linked glycosylation and lipid-linked oligosaccharide synthesis by stress responses in metazoan cells, Crit. Rev. Biochem. Mol. Biol. 41 (2006) 51–75. doi:10.1080/10409230500542575.

[13] J. Wu, S. Chen, H. Liu, Z. Zhang, Z. Ni, J. Chen, Z. Yang, Y. Nie, D. Fan, Tunicamycin specifically aggravates ER stress and overcomes chemoresistance in multidrug-resistant gastric cancer cells by inhibiting N-glycosylation, J. Exp. Clin. Cancer Res. 37 (2018) 272. doi:10.1186/s13046-018-0935-8.

[14] P. Guha, E. Kaptan, P. Gade, D. V Kalvakolanu, H. Ahmed, Tunicamycin induced endoplasmic reticulum stress promotes apoptosis of prostate cancer cells by activating mTORC1, Oncotarget. 8 (2017) 68191–68207. doi:10.18632/oncotarget.19277.

[15] L. Sun, Y. Zhao, K. Zhou, H.H. Freeze, Y.-W. Zhang, H. Xu, Insufficient ER-stress response causes selective mouse cerebellar granule cell degeneration resembling that seen in congenital disorders of glycosylation, Mol. Brain. 6 (2013) 52. doi:10.1186/1756-6606-6-52.

[16] M. Aebi, R. Bernasconi, S. Clerc, M. Molinari, N-glycan structures: recognition and processing in the ER, Trends Biochem. Sci. 35 (2010) 74–82. doi:https://doi.org/10.1016/j.tibs.2009.10.001.

[17] R. Raghunathan, J.D. Hogan, A. Labadorf, R.H. Myers, J. Zaia, A glycomics and proteomics study of aging and Parkinson's disease in human brain, Sci. Rep. 10 (2020) 1–9. doi:10.1038/s41598-020-69480-3.

[18] H. Wilkinson, K.A. Thomsson, A.L. Rebelo, M. Hilliard, A. Pandit, P.M. Rudd, N.G. Karlsson, R. Saldova, O-Glycome of Human Nigrostriatal Tissue and its Alteration in Parkinson's Disease, J. Proteome Res. (2021). doi:10.1021/acs.jproteome.1c00219.

[19] M. Frenkel-pinter, M.D. Shmueli, C. Raz, M. Yanku, S. Zilberzwige, E. Gazit, D. Segal, Interplay between protein glycosylation pathways in Alzheimer's disease, Sci. Adv. 3 (2017) 1–11. doi:10.1126/sciadv.1601576.

[20] G. Wu, Z.-H. Lu, N. Kulkarni, R.W. Ledeen, Deficiency of ganglioside GM1 correlates with Parkinson's disease in mice and humans, J. Neurosci. Res. 90 (2012) 1997–2008. doi:10.1002/jnr.23090.

[21] J. Lee, S. Ha, M. Kim, S.W. Kim, J. Yun, S. Ozcan, H. Hwang, I.J. Ji, D. Yin, M.J. Webster, C.S. Weickert, J.H. Kim, J.S. Yoo, R. Grimm, S. Bahn, H.S. Shin, H.J. An, Spatial and temporal diversity of glycome expression in mammalian brain, Proc. Natl. Acad. Sci. U. S. A. 117 (2020) 28743–28753. doi:10.1073/pnas.2014207117.

[22] S.E. Williams, M. Noel, S. Lehoux, M. Cetinbas, R.J. Xavier, R.I. Sadreyev, E.M. Scolnick, J.W. Smoller, R.D. Cummings, R.G. Mealer, Mammalian brain glycoproteins exhibit diminished glycan complexity compared to other tissues, Nat. Commun. 13 (2022). doi:10.1038/s41467-021-27781-9.

[23] A.L. Rebelo, P. Contessotto, K. Joyce, M. Kilcoyne, An optimized protocol for combined fluorescent lectin

/ immunohistochemistry to characterize tissue-specific glycan distribution in human or rodent tissues, Star Protoc. 1 (2021). doi:10.1016/j.xpro.2020.100237.

[24] J. Samal, R. Saldova, P.M. Rudd, A. Pandit, R.O. Flaherty, Region-specific characterization of N -glycans in striatum and substantia nigra of an adult rodent brain, Anal. Chem. (2020). doi:10.1021/acs.analchem.0c01206.

[25] A.C. Russell, M. Šimurina, M.T. Garcia, M. Novokmet, Y. Wang, I. Rudan, H. Campbell, G. Lauc, M.G. Thomas, W. Wang, The N-glycosylation of immunoglobulin G as a novel biomarker of Parkinson's disease, Glycobiology. 27 (2017) 501–510. doi:10.1093/glycob/cwx022.

[26] L. Veillon, C. Fakih, H. Abou-El-Hassan, F. Kobeissy, Y. Mechref, Glycosylation changes in brain cancer, ACS Chem. Neurosci. 9 (2018) 51–72. doi:10.1021/acschemneuro.7b00271.

[27] E.P. Demina, W.C. Pierre, A.L.A. Nguyen, I. Londono, B. Reiz, C. Zou, R. Chakraberty, C.W. Cairo, A. V Pshezhetsky, G.A. Lodygensky, Persistent reduction in sialylation of cerebral glycoproteins following postnatal inflammatory exposure, J. Neuroinflammation. 15 (2018) 336. doi:10.1186/s12974-018-1367-2.

[28] C. Klaus, H. Liao, D.H. Allendorf, G.C. Brown, H. Neumann, Sialylation acts as a checkpoint for innate immune responses in the central nervous system, Glia. 69 (2021) 1619–1636. doi:10.1002/glia.23945.

[29] H. Hildebrandt, A. Dityatev, Polysialic Acid in Brain Development and Synaptic Plasticity, Top Curr Chem. 266 (2015) 55-96. doi:10.1007/128.

[30] A. Regnier-Vigouroux, The mannose receptor in the brain, Int. Rev. Cytol. 226 (2003) 321–342. doi:10.1016/s0074-7696(03)01006-4.

[31] D. Matuskey, S. Tinaz, K.C. Wilcox, M. Naganawa, T. Toyonaga, M. Dias, S. Henry, B. Pittman, J. Ropchan, N. Nabulsi, I. Suridjan, R.A. Comley, Y. Huang, S.J. Finnema, R.E. Carson, Synaptic Changes in Parkinson Disease Assessed with in vivo Imaging, Ann. Neurol. 87 (2020) 329–338. doi:10.1002/ana.25682.

[32] B. Lössner, R. Jork, M. Lindner, B. Lucke, H. Matthies, Dopamine stimulated glycosylation of brain proteins in vitro is inhibited only partially by dopamine receptor antagonists., Biomed. Biochim. Acta. 43 (1984) 775–787.

[33] M. Schneider, E. Al-sharef, R.S. Haltiwanger, Biological functions of fucose in mammals, Glycobiology. 27 (2017) 601–618. doi:10.1093/glycob/cwx034.

[34] W. Gu, T. Fukuda, T. Isaji, Q. Hang, H. Lee, S. Sakai, J. Morise, J. Mitoma, H. Higashi, N. Taniguchi, H. Yawo, S. Oka, J. Gu, Loss of alpha1,6-fucosyltransferase decreases hippocampal long term potentiation: implications for core fucosylation in the regulation of AMPA receptor heteromerization and cellular signaling, J. Biol. Chem. 290 (2015) 17566–17575. doi:10.1074/jbc.M114.579938.

[35] X. Lu, D. Zhang, H. Shoji, C. Duan, G. Zhang, T. Isaji, Deficiency of α1,6-fucosyltransferase promotes neuroinflammation by increasing the sensitivity of glial cells to inflammatory mediators, Biochim. Biophys. Acta. 1863 (2018) 598–608. doi:10.1016/j.bbagen.2018.12.008.

[36] Y.J. Chen, D.R. Wing, G.R. Guile, R. a Dwek, D.J. Harvey, S. Zamze, Neutral N-glycans in adult rat brain tissue-complete characterisation reveals fucosylated hybrid and complex structures, Eur. J. Biochem. 251 (1998) 691–703. doi:10.1046/j.1432-1327.1998.2510691.x.

[37] R. Aalinkeel, S.D. Mahajan, Neuroprotective role of galectin-1 in central nervous system pathophysiology, Neural Regen. Res. 11 (2016) 896–897. doi:10.4103/1673-5374.184455.

[38] Z. Ye, J.D. Marth, N-glycan branching requirement in neuronal and postnatal viability, Glycobiology. 14 (2004) 547–568. doi:10.1093/glycob/cwh069.

[39] K. Akasaka-manya, H. Manya, Y. Sakurai, B.S. Wojczyk, Y. Kozutsumi, Y. Saito, N. Taniguchi, S. Murayama, S.L. Spitalnik, T. Endo, Protective effect of N-glycan bisecting GlcNAc residues on β-amyloid production in Alzheimer's disease, Glycobiology. 20 (2010) 99–106. doi:10.1093/glycob/cwp152.

[40] T.R. Hawkinson, H.A. Clarke, L.E.A. Young, L.R. Conroy, K.H. Markussen, K.M. Kerch, L.A. Johnson, P.T. Nelson, C. Wang, D.B. Allison, M.S. Gentry, R.C. Sun, In situ spatial glycomic imaging of mouse and human Alzheimer's disease brains, Alzheimer's Dement. (2021) 1–15. doi:10.1002/alz.12523.

[41] M.Y. Wong, K. Chen, A. Antonopoulos, B.T. Kasper, M.B. Dewal, R.J. Taylor, C.A. Whittaker, P.P. Hein, A. Dell, J.C. Genereux, S.M. Haslam, L.K. Mahal, M.D. Shoulders, XBP1s activation can globally remodel N-glycan structure distribution patterns, Proc. Natl. Acad. Sci. 115 (2018) E10089–E10098. doi:10.1073/pnas.1805425115.

[42] E.J. Ryu, H.P. Harding, J.M. Angelastro, O. V Vitolo, D. Ron, L.A. Greene, Endoplasmic reticulum stress and the unfolded protein response in cellular models of Parkinson's disease, J. Neurosci. 22 (2002) 10690–10698.

[43] B. Ning, Q. Zhang, M. Deng, N. Wang, Y. Fang, Endoplasmic reticulum stress induced autophagy in 6-OHDA-induced Parkinsonian rats, Brain Res. Bull. 146 (2019) 224–227.

doi:10.1016/j.brainresbull.2019.01.001.

[44] J.J.M. Hoozemans, E.S. van Haastert, P. Eikelenboom, R.A.I. de Vos, J.M. Rozemuller, W. Scheper, Activation of the unfolded protein response in Parkinson's disease, Biochem. Biophys. Res. Commun. 354 (2007) 707–711. doi:10.1016/j.bbrc.2007.01.043.

[45] T. Higuchi, Y. Watanabe, I. Waga, Protein disulfide isomerase suppresses the transcriptional activity of NF-kappaB, Biochem. Biophys. Res. Commun. 318 (2004) 46–52. doi:10.1016/j.bbrc.2004.04.002.

[46] M. Wang, S. Wey, Y. Zhang, R. Ye, A.S. Lee, Role of the unfolded protein response regulator GRP78/BiP in development, cancer, and neurological disorders., Antioxid. Redox Signal. 11 (2009) 2307–2316. doi:10.1089/ars.2009.2485.

[47] N. Egawa, K. Yamamoto, H. Inoue, R. Hikawa, K. Nishi, K. Mori, R. Takahashi, The endoplasmic reticulum stress sensor, ATF6α, protects against neurotoxin-induced dopaminergic neuronal death, J. Biol. Chem. 286 (2011) 7947–7957. doi:10.1074/jbc.M110.156430.

[48] W.F.I. Glass, R.C. Briggs, L.S. Hnilica, Use of lectins for detection of electrophoretically separated glycoproteins transferred onto nitrocellulose sheets., Anal. Biochem. 115 (1981) 219–224. doi:10.1016/0003-2697(81)90549-2.

[49] J.C. Bigge, T.P. Patel, J.A. Bruce, P.N. Goulding, S.M. Charles, R.B. Parekh, Nonselective and efficient fluorescent labeling of glycans using 2-amino benzamide and anthranilic acid, Anal. Biochem. 230 (1995) 229–238. doi:10.1006/abio.1995.1468.

[50] L. Royle, C.M. Radcliffe, R.A. Dwek, P.M. Rudd, Detailed structural analysis of N-glycans released from glycoproteins in SDS-PAGE gel bands using HPLC combined with exoglycosidase array digestions, Methods Mol. Biol. 347 (2006) 125–143. doi:10.1385/1-59745-167-3:125.

[51] L. Royle, M.P. Campbell, C.M. Radcliffe, D.M. White, D.J. Harvey, J.L. Abrahams, Y.-G. Kim, G.W. Henry, N.A. Shadick, M.E. Weinblatt, D.M. Lee, P.M. Rudd, R.A. Dwek, HPLC-based analysis of serum N-glycans on a 96-well plate platform with dedicated database software, Anal. Biochem. 376 (2008) 1–12. doi:10.1016/j.ab.2007.12.012.

[52] A.L. Rebelo, F. Gubinelli, P. Roost, C. Jan, E. Brouillet, N. Van Camp, R.R. Drake, R. Saldova, A. Pandit, Complete spatial characterisation of N-glycosylation upon striatal neuroinflammation in the rodent brain, J. Neuroinflammation. 18 (2021) 1–19. doi:10.1186/s12974-021-02163-6.

[53] P.M. Angel, A. Mehta, K. Norris-Caneda, R.R. Drake, MALDI Imaging Mass Spectrometry of N-glycans and Tryptic Peptides from the Same Formalin-Fixed, Paraffin-Embedded Tissue Section, Methods Mol. Biol. 1788 (2018) 225–241. doi:10.1007/7651_2017_81.

FIGURES

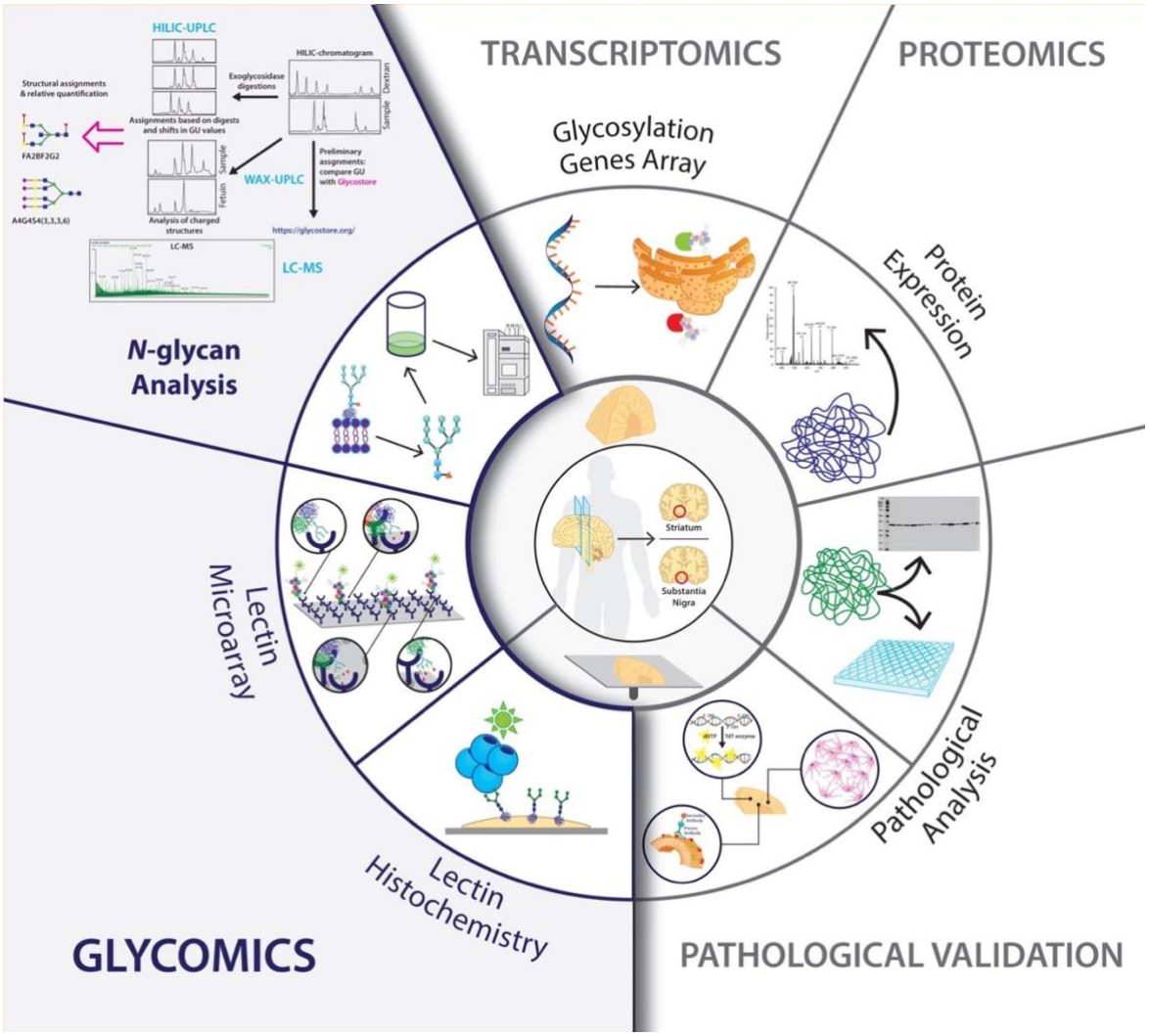

Figure 1. Schematic representation of the experimental design and procedures followed in this chapter. The study was designed for the spatial and temporal characterisation of the molecular signature in the Parkinsonian brain, with a focus on *N*-glycosylation. Two regions were analysed (striatum and substantia nigra) from healthy subjects (n=18), Incidental Lewy-Body Disease (ILBD) patients (n=3) and Stage 3-4 Parkinson's Disease (PD) patients (n=15). Brain tissue from these patients was acquired either snap-frozen or in fixed-frozen sections. For the *N*-glycome studies, a multi-faceted approach was developed using Hydrophilic Interaction Ultra Performance Liquid Chromatography (HILIC-UPLC), exoglycosidase digestions, Weak Anion Exchange Liquid Chromatography (WAX-UPLC) and Liquid Chromatography-Mass Spectrometry (LC-MS). Snap frozen tissue was used to perform glycomic, transcriptomic and proteomic analyses. Sections were used to validate the previous findings through Matrix-Assisted Laser Desorption/Ionisation Mass Spectrometry Imaging (MALDI MSI), and fluorescent and chromogenic histochemistry stainings.

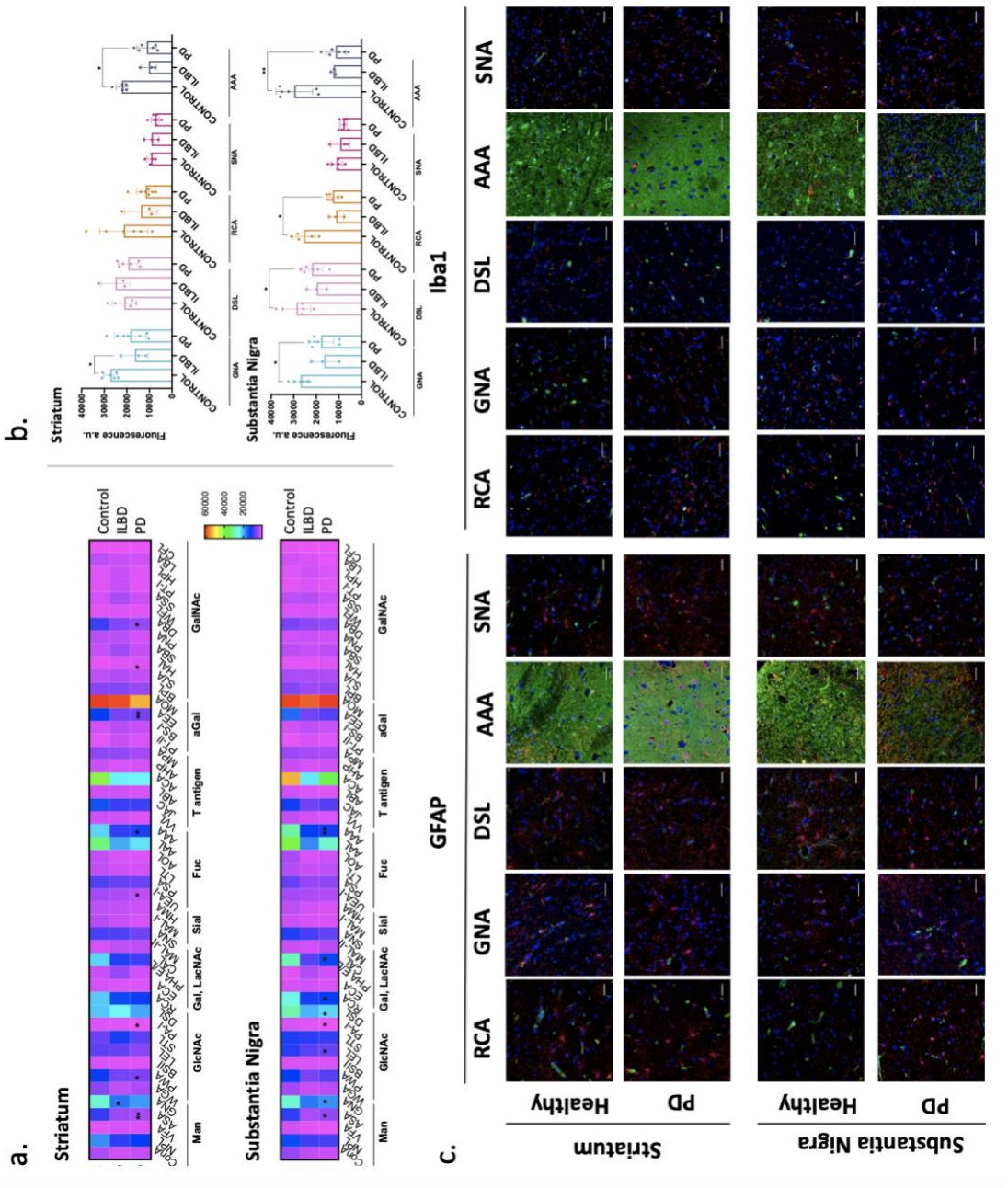

Figure 2 Overall changes in striatal and nigral tissue glycosylation upon Parkinson's Disease. a. Lectin array assay performed on the protein lysate obtained from healthy (n=7), ILBD patients (n=3) and PD patients (n=7) to detect the expression of individual glycan structures present on both *N*- and *O*-linked glycans. Data presented as the mean ± SD. Two-way ANOVA was performed followed by Tukey's post-hoc test and statistical significance set at *p<0.05 and **p<0.01 in relation to the healthy group. b. Relative expression of the main g differently regulated glycans in the tissue (as indicated in the lectin array). c. Combined lectin and immunohistochemistry was used to study the spatial distribution of the main differently regulated glycans in the tissue (as indicated in the lectin array), and to associate their expression with specific inflammation-related cell types – astrocytes (GFAP+) and microglia (Iba1+). Scale bar = 50 µm.

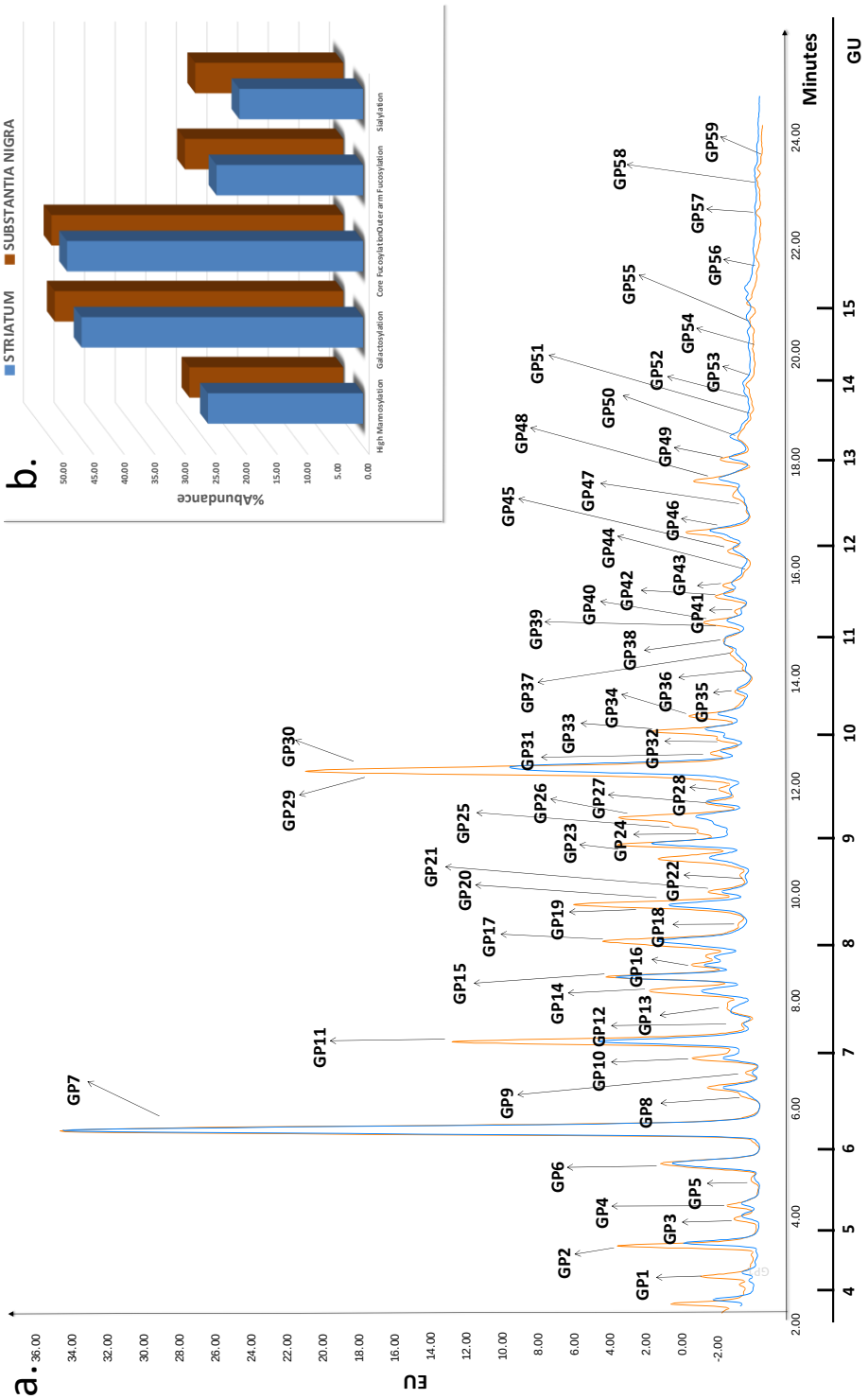

c.

Peak number	STRIATUM				Peak number	SUBSTANTIA NIGRA			
	HEALTHY		PD			HEALTHY		PD	
GP	Structure	Peak Area (%)	Structure	Peak Area (%)	GP	Structure	Peak Area (%)	Structure	Peak Area (%)
1	M3	0.44	M3	0.37	1	M3	0.49	M3	0.43
2	F(6)M3	2.11	F(6)M3	1.53	2	F(6)M3	1.70	F(6)M3	1.76
3	M4	0.43	M4	0.46	3	M4	0.42	M4	0.44
4	F(6)A1	0.48	F(6)A1	0.53	4	F(6)A1	0.51	F(6)A1	0.59
5	A2B	0.78	A2B	0.20	5	M4A1	0.32	M4A1	0.31
6	A3	2.57	A3	2.53	6	F(6)A2	2.29	A3/F(6)A2	2.27
7	F(6)A3 (M5)	20.46	F(6)A3 (M5)	21.09	7	F(6)A3 (M5)	19.01	F(6)A3 (M5)	18.74
8	F(6)M5	1.21	F(6)M4A1B	1.19	8	F(6)M4A1B	1.16	F(6)M5	1.24
9	M5A1	0.15	A4B	0.16	9	A4B	0.15	A2G1GalNAc1S(3)1 (SO4- on GalNAc)	0.17
10	F(6)A4	1.05	F(6)A4	1.16	10	F(6)A4	1.08	F(6)A4	1.28
11	M6	5.09	M6	5.13	11	M6	5.81	M6	6.18
12	M5A2	0.40	M5A2	0.43	12	M5A2	0.35	A2F1G1GalNAc1	0.33
13	A3G(4)2/A3G(3)2	0.81	F(6)A2F1G(4)1	0.82	13	F(6)A2BG1	0.68	F(6)A4GalNAc1	0.62
14	M7/A4F1	1.79	M7	1.84	14	A3BG(4)2	2.02	F(6)A2G(3)2/F(6)A2G(4)2	2.07
15	F(6)A2BF1G1	3.89	F(6)A3F1G1/F(6)A2BF1G1	3.98	15	F(6)M5A2	3.37	F(6)A3F1G1/F(6)A2BF1G1	3.09
16	M7	1.46	F(6)A3F1G1	1.55	16	M7	1.36	M7/F(6)A2F1G1GalNAc1	1.35
17	M7	4.42	M7	4.42	17	M7	4.68	M7	4.72
18	F(6)A4BF1	0.95	F(6)A4GalNAc2	1.03	18	F(6)A2BG1S(3)1	0.92	M7	0.91
19	A3F3	1.18	A3F3	1.41	19	F(6)A4F1GalNAc1	1.29	F(6)A4F1GalNAc1	1.56
20	A3G(4)3	1.09	A2G2S(3)1	0.90	20	A2G2S(3)1	1.27	A2G2S(3)1	1.09
21	F(6)A4G1Lac1	1.12	F(6)A3BF1G(4)1	1.12	21	F(6)M7	1.02	A3F1G1Sg(6)1	0.98
22	A3BG(3)3/A3BG(4)3	0.50	A3BG(3)3/A3BG(3)3	0.52	22	A3BG(3)3	0.48	F(6)A2G(4)2S(3)1	0.51
23	M8	4.15	M8	4.30	23	M8	4.50	M8	4.35
24	M8	0.46	M8	0.51	24	M8	0.44	F(6)A4F2G(3)4	0.35
25	F(6)A3BG(4)3	0.95	F(6)A4F1G2	0.98	25	F(6)A3BG(4)3/A4F2G1	1.00	M8	1.02
26	F(6)A2BF2G2	1.85	F(6)A2BF2G2	1.90	26	F(6)A3F2G1S(3)1/F(6)A3F2G1S(6)1	2.02	F(6)A3F2G1S(3)1	1.89
27	A3BF2G1S(3)2/A3BF2G1S(6)2	1.86	F(6)A4F3	1.95	27	F(6)A4F3	1.72	A3BF2G1S(6)2	1.44
28	A4G(3)3Lac1/A4G(4)3Lac1	0.93	F(6)A2F2G2GalNAc1	0.89	28	F(6)A3G2Gal2	0.88	A4G(3)3Lac1/A4G(4)3Lac1	0.81
29	M9	5.05	M9	5.43	29	M9	5.31	M9	4.84
30	A2G2S(6)2	3.17	A2G2S(3)2	3.13	30	A2G2S(6)2	3.66	F(6)A2G(4)2S(3,6)2	3.87
31	F(6)A4G3Lac1	0.98	A3F1G1Gal2GalNAc1	1.05	31	A4G(4)4/A4G(3)4	1.06	A4G(4)4	1.21
32	F(6)A3G3S(3)1	0.64	N/A	0.61	32	FA4F1GalNAc1S(6,8)2	0.66	F(6)A3G3S(3)1	0.55
33	F(6)A2F2G2S(6)1	1.77	A4BG3S(3)1	1.81	33	A4F2G2	1.71	A4BG(3)4	1.57
34	F(6)A4F3G1	1.08	F6)A3G2Lac2	0.94	34	F(6)A4F3G(4)1	0.99	F(6)A4F3G1	0.96
35	F(6)A3BG2Lac2	0.78	F(6)A4G(4)4	0.85	35	A3BG3S(6)2	0.81	F(6)A4G2Sg(6)1	0.74
36	F(6)A4F1G(3)3	0.43	F(6)A4F1G(3)3	0.44	36	F(6)A4F1G3	0.40	F(6)A4F1G3	0.29
37	A4G(3)4Gal1	0.52	A4G3GlcNAc3	0.54	37	A4G4Gal1	0.51	A4G(4)4Gal1	0.55
38	M10	2.20	F(6)A3G3S(3)2	2.28	38	F(6)A3G3S(6)2	1.97	F(6)A3F2G(3)3/F(6)A3F2G(4)3	1.78
39	F(6)A3BG3GlcNAc2S(3,6)2/ F(6)A3BG3GlcNAc2S(6)2	0.78	F(6)A4F3GalNAc3	0.65	39	A4BF3G1S(6)1	1.05	A4BF3G1S(6)1	1.07
40	F(6)A4BF4G1	0.71	F(6)A4BF4G1	0.79	40	F(6)A4BF4G1	0.81	F(6)A4BF4G1	0.93
41	F(6)A4G4Gal1	0.47	F(6)A4G(4)4Gal1	0.45	41	F(6)A4G(4)4Gal1/F(6)A4G(3)4Gal1	0.57	F(6)A4F3GalNAc4	0.63
42	M11	0.97	A3F1G1Gal2S(3)2/A3F1G1Gal2S(6)2	1.02	42	M11	1.04	F(6)A4G2Sg(3)2	1.01
43	A3F1G1Gal2S(3)3	1.00	F(6)A4F1G2S(6)2	1.00	43	A3F1G1Gal2S(3)3	1.00	A3F1G1Gal2S(3)3	1.11
44	F(6)A3F1G2Sg(3,3,8)3	0.35	F(6)A3F1G2Sg(3,3,8)3	0.41	44	A4F3G4	0.30	A4F3G(4)4	0.22
45	F(6)A4G(3)4Lac1Gal1/ F(6)A4G(4)4Lac1Gal1	1.38	F(6)A4F3G1Sg(3)1	1.35	45	F(6)A4G(3)4Lac1Gal1/ F(6)A4G(4)4Lac1Gal1	1.42	F(6)A4G3Lac1Gal1	1.66
46	F(6)A4F3G3	1.60	A4BG3S(6)1Sg(6)1	1.51	46	F(6)A3BF1G2S(3,6,8)3,F(6)A3BF1G2S(3,3,8)3	2.10	F(6)A3BF1G2S(3,3,8)3/F(6)A3BF1G2S(6,6,8)3	1.49
47	A4BF3G3	0.36	A4BG3Lac1GlcNAc2S(3)1	0.32	47	F(6)A3F2G1S(3,8,8,8)4	0.80	F(6)A4F3G1S(6,8)2	1.22
48	F(6)A4F3G4	2.20	F(6)A4F(2)3G(4)4	2.17	48	F(6)A2G2Gal2Sg(6)2	1.94	F(6)A2G2Gal2Sg(6)2/F(6)A4F1G3S(3)3/ F(6)A4F1G3S(6)3	2.26
49	A3F1G(4)3S(6)2Sg(3)1	1.18	F(6)A3BG3Sg(6)2	1.08	49	A3F(3)1G(4)3S(6)2Sg(3)1	1.81	A3F(3)1G(4)3S(6)2Sg(3)1	1.54
50	A4G4S(3)4	0.40	A4G4S(3)4	0.39	50	F(6)A4BF4G1Sg(6)1/A4BF3G1S(3,8,8)3	1.99	A4G4S(3)4/F(6)A4BF4G1Sg(3)1	0.57
51	F(6)A4G(3)4Lac3/F(6)A4G(4)4Lac3	2.15	A4BF3G3GalNAc2	2.13	51	A4F4G(4)4S(3)1	0.41	A4F4G(4)4S(3)1	2.43
52	F(6)A4G4S(3)4	0.81	F(6)A4G4S(6)4	0.83	52	F(6)A4G4S(3)4 /F(6)A4G4S(6)4	0.78	A4G(3)4Gal1GalNAc2S(3)2/A4G(3)4Gal1GalNAc2S(6)2	0.65
53	A4BG4S(3)3/A4BG4S(6)3	0.82	A4BG4S(6)3	0.83	53	A4BG4S(3)3/A4BG4S(6)3	0.87	A4BG4S(3)3/A4BG4S(6)3	0.96
54	A4F3G4S(3)4/A4F3G4S(6)4	1.35	A4F3G4S(3)4/A4F3G4S(3,6,6,6,6)4/ A4F3G4S(6)4	1.33	54	A4F3G4S(6)4	1.19	A4F3G4S(6)4	1.04
55	F(6)A4BF4G2Gal3	0.29	F(6)A4BF4G2Gal3	0.25	55	F(6)A4G4Lac4Gal1	0.25	F(6)A4G4Lac4Gal1	0.43
56	F(6)A4G4Lac3S(6)2	1.58	F(6)A4G4Lac3S(3)2	1.55	56	F(6)A4F3G4S(3,3,6)3/F(6)A4F3G4S(6)3	1.45	F(6)A4G4Lac3S(3)2	1.33
57	A2G2S(6,6,8,8)4	0.40	A2G2S(6,6,8,8)4	0.41	57	A2G2S(6,6,8,8)4	0.40	A2G2S(6,6,8,8)4	0.40
58	F(6)A4BF2G3S(6)3	0.45	F(6)A4F3GalNAc1S(6,8,8,8)4	0.37	58	F(6)A4BF2G(4)3S(6)3	0.42	F(6)A4F2G4S(6)1Sg(3)4	1.11
59	F(6)A4F2G4Sg(3)4S(8)1	0.57	A4BF3G4S(6)4	0.54	59	A4G4Gal1GalNAc2S(6)4	0.69	A4G4Gal1GalNAc2S(6)4	0.06

d.

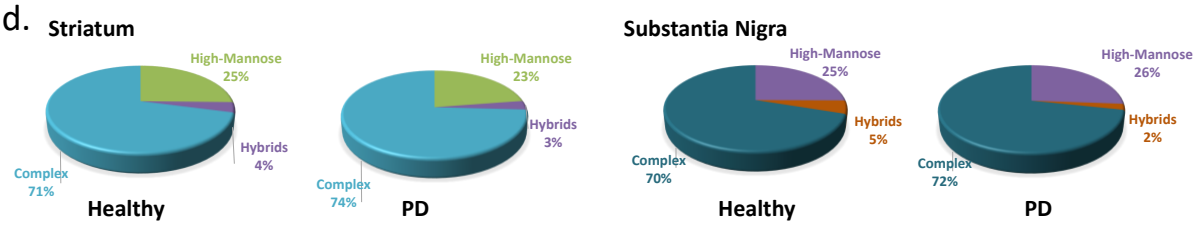

Figure 3. *N*-glycome in healthy and PD human nigro-striatal regions. a. HILIC-UPLC chromatograms obtained for both human striatum (blue profile) and substantia nigra (orange profile). The *N*-glycome for both these regions was separated into 59 chromatographic peaks (GP). EU – emission units. b. Abundance of the main glycosylation traits present in the healthy striatum and substantia nigra. c. Summary of the detailed composition analysis for each of these peaks, indicating the major glycan structure present in each peak and the peak area. d. Abundance of the three general types of *N*-glycans (hybrid, complex and high mannose) in both the striatum and substantia nigra, in healthy and PD samples.

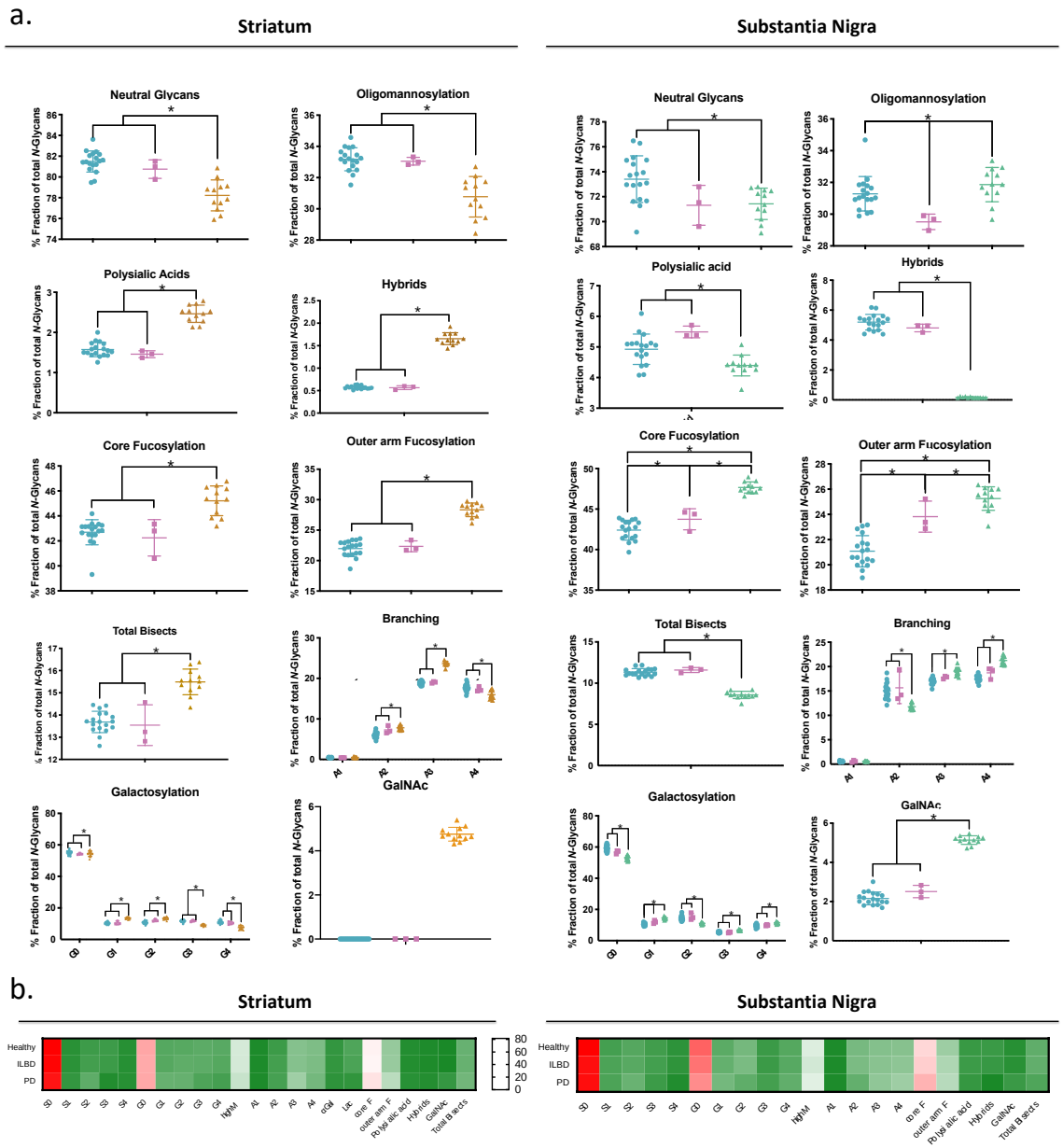

Figure 4. Changes in the *N*-glycosylation traits in the different regions and different disease stages. a. The common glycosylation features amongst the main structures in each glycan peak were grouped in the main glycosylation traits (according to Table 2.5). The abundance of these was log transformed. Data is presented as mean ± SD. One-way ANOVA was performed since the data was shown to be normally distributed. This was followed by Tukey's post-hoc test and statistical significance set at *p<0.05. Blue: healthy; Pink: ILBD; Yellow/Green: PD. b. Differences seen in terms of abundance amongst the main glycosylation traits.

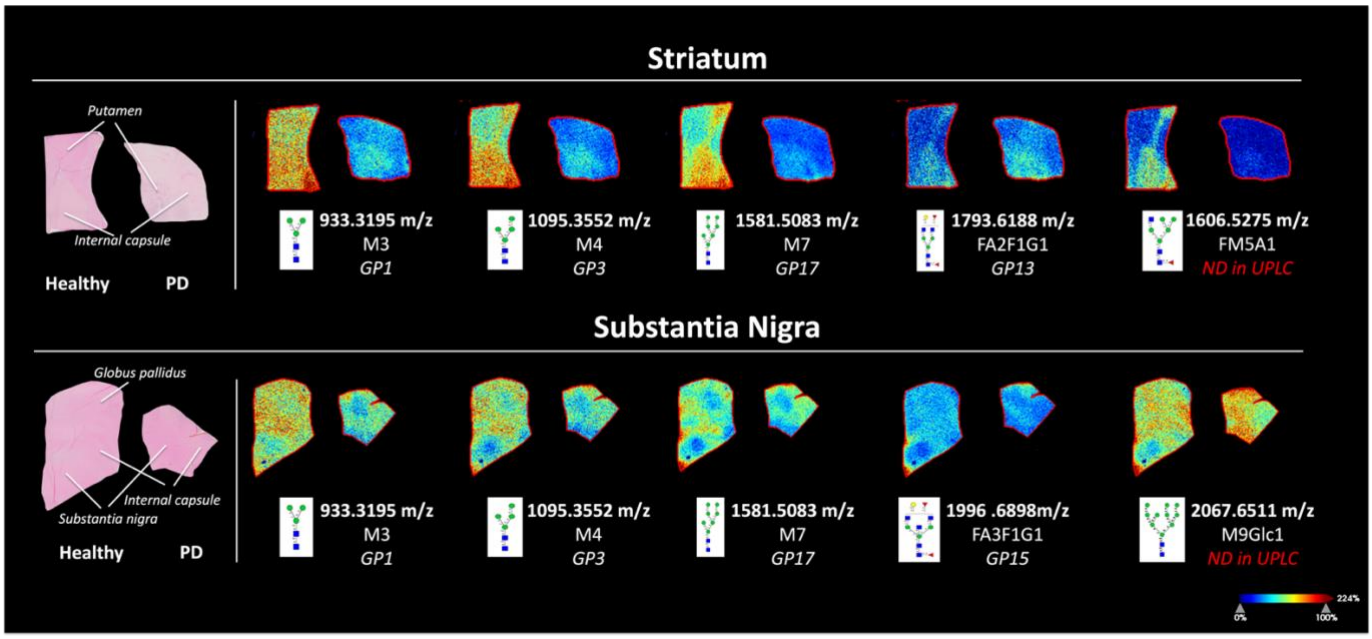

Figure 5. *N*-glycan imaging of the main structures differently regulated in the striatum and substantia nigra of PD and age-matched control human brains. Each image is accompanied by the putative structures determined by combinations of accurate m/z, CID fragmentation patterns and glycan database structure. ND – non-detected

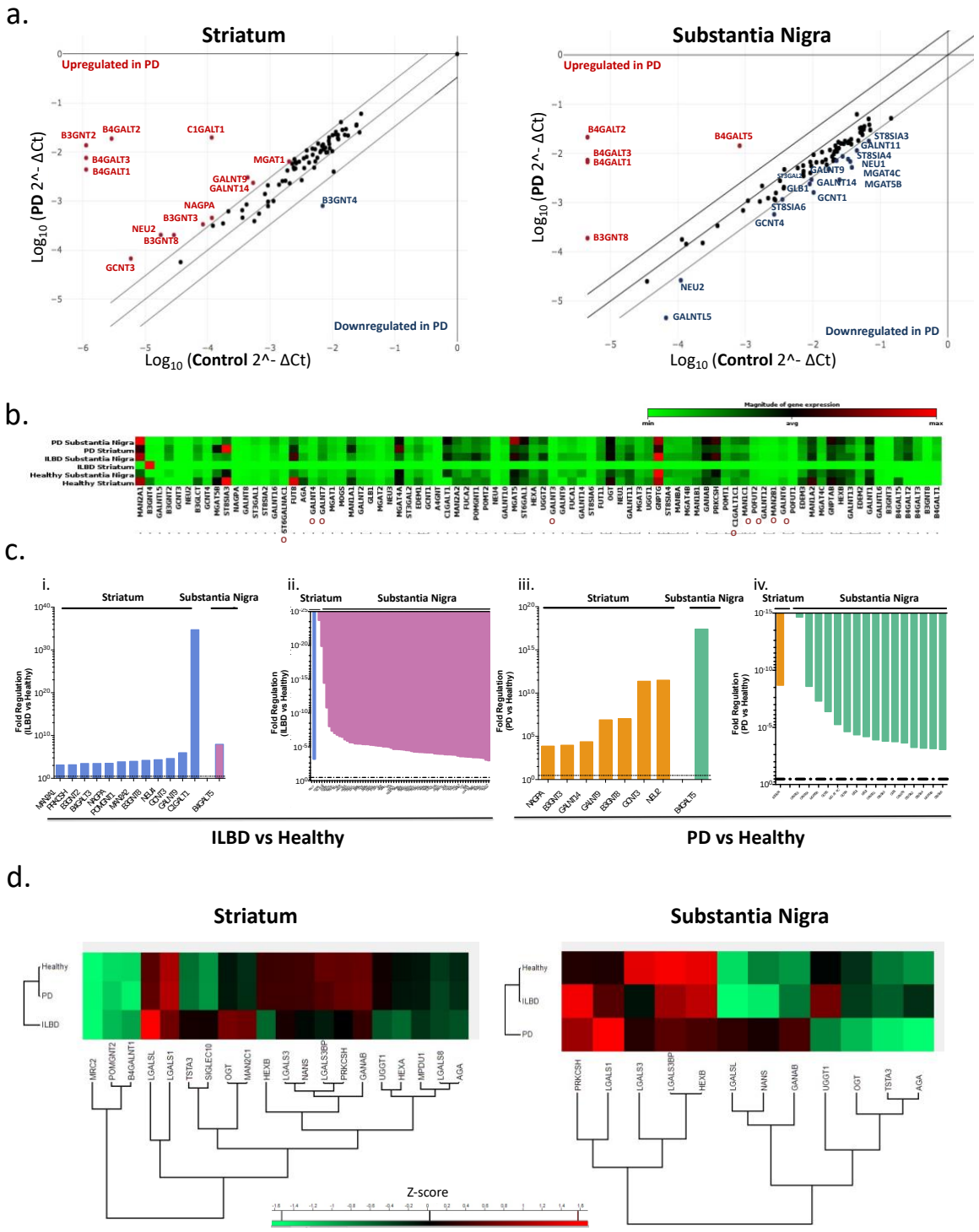

Figure 6. Expression of the human nigro-striatal glycoenzymes upon Incidental Lewy Bodies Disease and Parkinson's Disease. a. Expression of 84 transcripts of glycosylation enzymes was performed using RT² Profiler™ PCR Array - Human Glycosylation (Qiagen®) and analysed through the GeneGlobe Data Analysis Center®. Significant upregulation (indicated in red) or downregulation (indicated in blue) of the different genes was considered when fold change ≥ 3 and $p \leq 0.05$. **b.** Relative expression of each transcript in healthy, ILBD and PD samples. Red indicates high relative expression and green low

relative expression. Expression levels were normalised on the house keeping gene GAPDH. **O** indicated enzymes involved only in *O*-glycosylation. All the others are involved only in *N*-glycosylation or in both types of glycosylation. **c.** Genes significantly upregulated (i., iii.) or downregulated (ii., iv.) in ILBD (i., ii.) and in PD (iii., iv.) conditions, in both the striatum and substantia nigra (considered when fold change ≥ 3 . Data represents the pool of mRNA from six biological replicates for the healthy group, three for ILBD group and six for PD group. **d.** Relative expression of the glycoenzymes detected by proteomics (through nanoLC-MS) in health, ILBD and PD samples according to their z-score (red: upregulated proteins, and green: downregulated proteins).

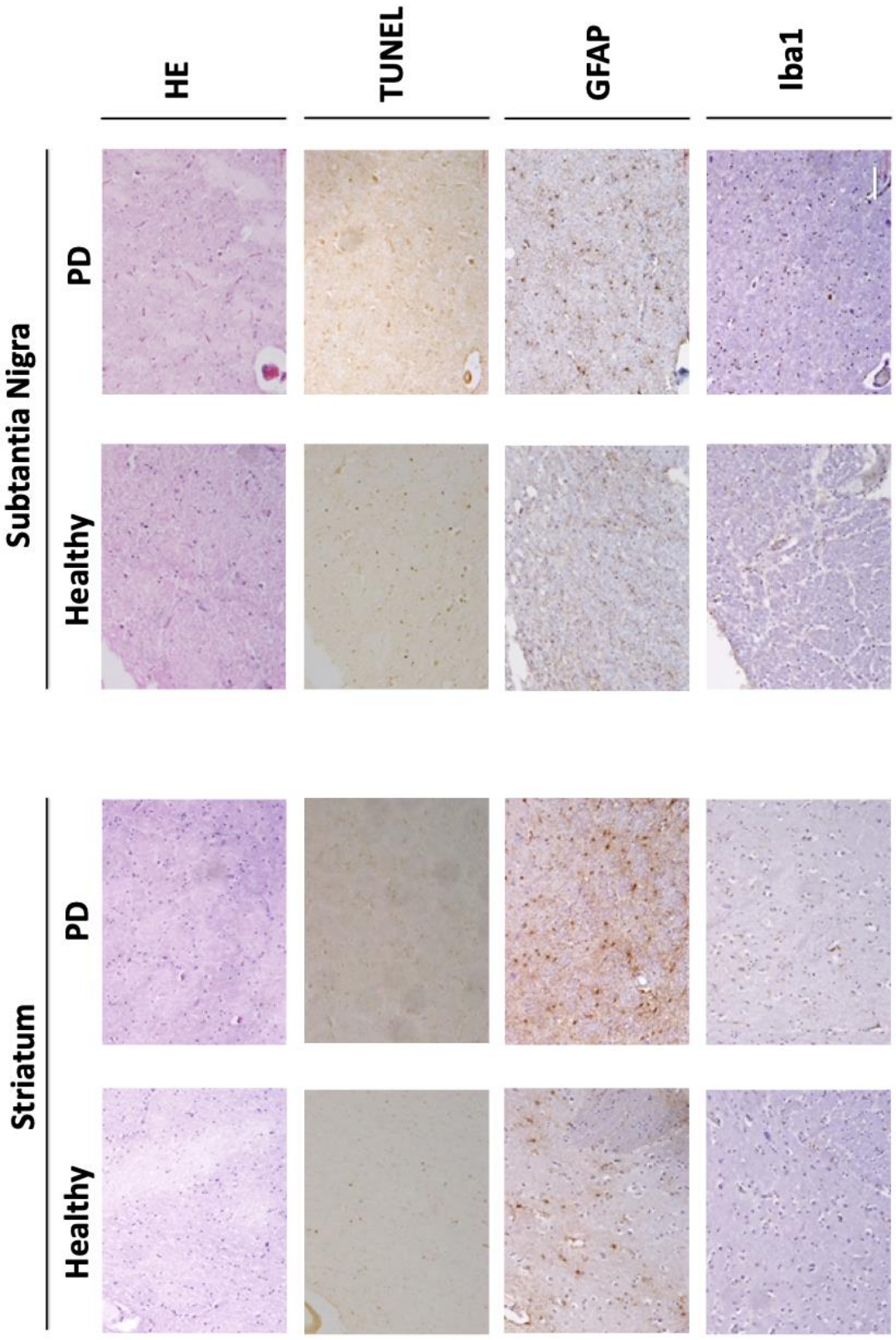

a.

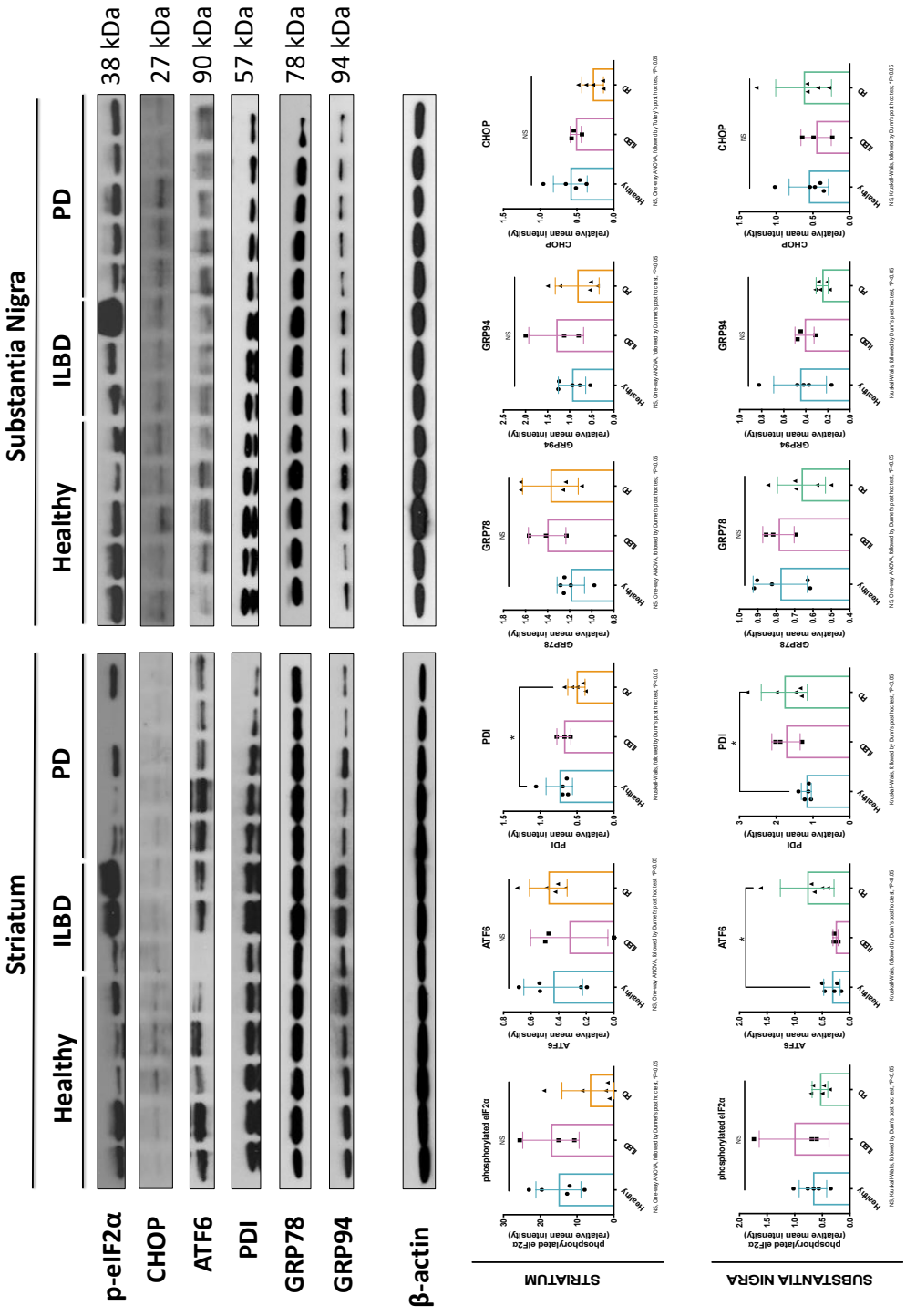

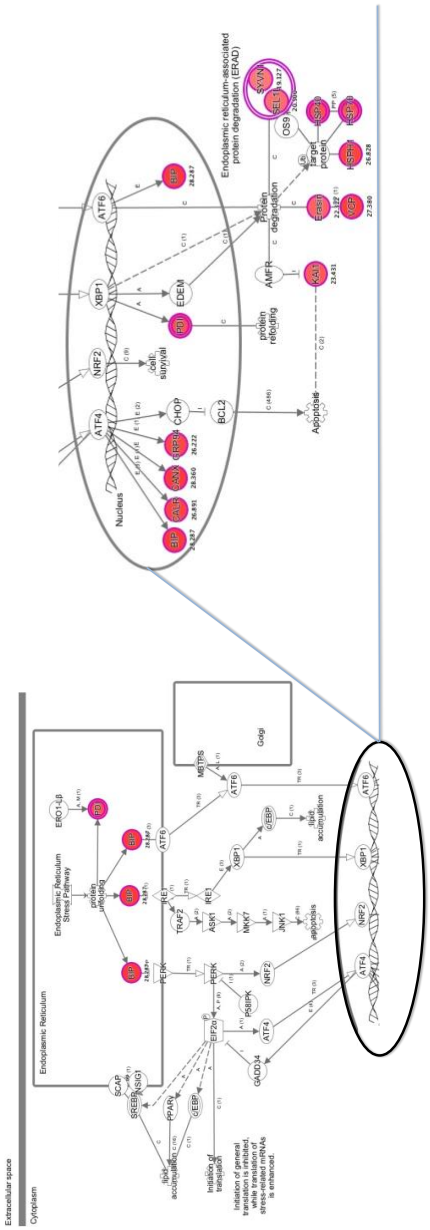

ن

Figure 7. Pathological markers regulation upon PD in the striatum and substantia nigra with a focus on the endoplasmic reticulum stress (ER stress) and unfolded protein response (UPR). a. Morphological characterisation and spatial analysis of the distribution of the main neuroinflammation-related cells in both the striatum and substantia nigra upon PD. (i) Heamatoxylin/Eosin (H&E) staining, (ii) terminal deoxynucleotidyltransferase dUTP nick end labelling (TUNEL) staining, (iii) anti-GFAP (astrocytes marker) immunohistochemistry, (iv) anti-Iba1 (microglia marker) immunohistochemistry. Scale bar = 100 µm. **b.** Expression of ER stress/UPR related markers (GRP78, GRP94, PDI, ATF6, phosphorylated eIF2a, CHOP) was assessed and quantified through western blot analysis. If the data was normally distributed, one-way ANOVA was performed and

followed by Dunnett post-hoc test, and statistical significance set at *p<0.05. If the data was not normally distributed, Kruskall-Wallis test followed by Dunn's post hoc test were carried out, and statistical significance was set at *p<0.05. **c.** Ingenuity Pathway Analysis (IPA) of canonical 'unfolded protein response' in Parkinsonian substantia nigra, based on the proteomic analysis performed after running the proteins in nanoLC-MS. Red symbols indicate identified and upregulated activation of proteins in the signalling pathway from a diseased brain associated with ER stress.

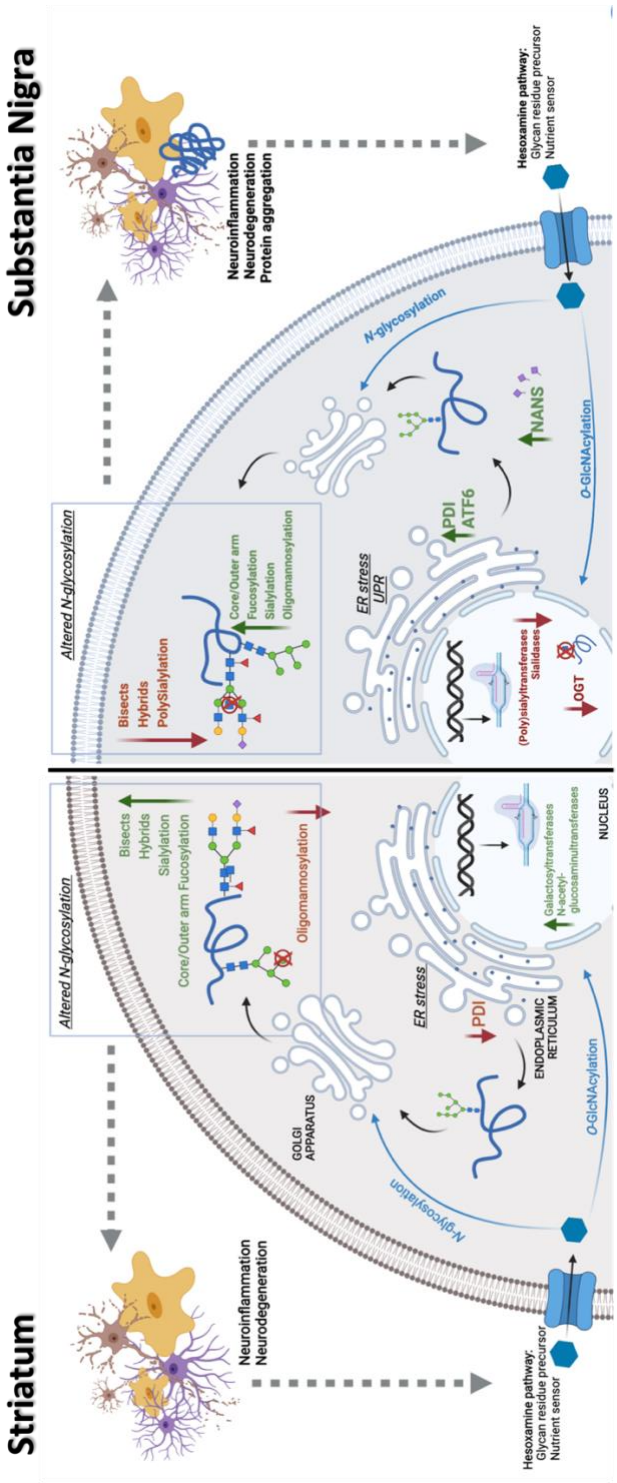

Figure 8. Summary and main conclusions seen regarding the molecular signature in each brain region upon PD. Differential regulation of glycosylation traits, glycosylation enzymes and UPR-related proteins is seen in the striatum vs substantia nigra. Created with BioRender®.

AUTHOR INFORMATION

Corresponding Author

*Abhay Pandit, abhay.pandit@nuigalway.ie

Author Contributions

A.L. Rebelo performed all the experiments except the lectin array. R. R. Drake developed the method for MALDI imaging of *N*-glycans. M.Marchetti-Deschmann supervised the *N*-glycan characterisation and analysis through MALDI imaging. R. Saldova managed and supervised the *N*-glycan characterisation and analysis through liquid chromatography and mass spectrometry. A. Pandit supervised, managed the overall study and secured funding. A.L. Rebelo wrote the manuscript, which was edited and approved by all co-authors.

ABREVIATIONS

ATF6: activating transcription factor 6

CNS: Central nervous system

DMB: 1,2-diamino-4,5-methylenedioxybenzene Dihydrochloride

ER: Endoplasmic reticulum

ERAD: Endoplasmic reticulum associated protein degradation

GFAP: Glial fibrillary acidic protein

GRP78: heat shock protein 70, binding immunoglobulin protein (BiP)

GRP94: heat shock protein 90

HBP: Hexosamine biosynthetic pathway

HILIC-UPLC: Hydrophilic Interaction Liquid Chromatography - Ultra Performance Liquid Chromatography

Iba1: Ionized calcium binding adaptor molecule 1

ILBD: Incidental Lewy body disease

IRE1: Inositol requiring enzyme 1

LC-MS: Liquid chromatography-mass spectrometry

LLO: Lipid-linked oligosaccharide

PERK: Protein kinase-like endoplasmic reticulum kinase

PAS: periodic acid Schiff

PD: Parkinson's disease

PDI: Protein disulphide isomerase

UHPLC: Ultra-High Performance Liquid Chromatography

UGGT: UDP-glucose:glycoprotein glucosyltransferase

UPR: Unfolded protein response

VGIC: voltage-gated ion channels

WAX-UPLC: Weak Anion Exchange - Ultra Performance Liquid Chromatography

ACKNOWLEDGMENTS

The authors would like to acknowledge the Parkinson's UK Brain Bank, funded by Parkinson's UK, a charity registered in England and Wales (258197) and in Scotland (SC037554) for supplying the tissue samples and associated clinical and neuropathological data. The authors are grateful to Mr Anthony Sloan and Dr Raghvendra Bohara for proof-reading this manuscript and Mr Maciej Doczyk for designing Figure 1. The authors are thankful to Ms Paula Kenny (from the National Institute for Bioprocessing Research and Training, Dublin, Ireland) for her help in performing the DMB analysis. The authors thank Mr Stefan Kirnbauer (from the Technical University of Vienna, Austria) for the help while establishing the method to acquire *N*-glycan detection through MALDI-MSI. The authors also acknowledge the facilities and scientific and technical assistance of the Centre for Microscopy & Imaging at the National University of Ireland Galway, facilities that are funded by NUI Galway, and the Irish Government's Programme for Research in Third-Level Institutions, Cycles 4 and 5, National Development Plan 2007–2013 (www.imaging.nuigalway.ie). Finally, the authors are thankful to DC

Proteomics (UK) for performing the proteomic analytical service and to Asparia Glycomics (San Sebastian, Spain) for providing the lectin microarray analytical service.

Funding Sources

This publication has emanated from research supported by a research grant from Science Foundation Ireland (SFI), co-funded under the European Regional Development Fund through Grant number 13/RC/2073 and 13/RC/2073_2, and by the BrainMatTrain project, which is funded by the European Union Horizon 2020 Programme (H2020-MSCA-ITN-2015) under the Marie Skłodowska-Curie Initial Training Network and Grant Agreement No. 676408.

Competing interests

The authors declare no conflict of interests.